

Wide-Field Feedback Neurons Dynamically Tune Early Visual Processing

John C. Tuthill,^{1,2} Aljoscha Nern,¹ Gerald M. Rubin,¹ and Michael B. Reiser^{1,*}

¹HHMI/Janelia Farm Research Campus, 19700 Helix Drive, Ashburn, VA 20147, USA

²Present address: Department of Neurobiology, Harvard Medical School, 220 Longwood Avenue, Boston, MA 02115, USA

*Correspondence: reisermb@janelia.hhmi.org

<http://dx.doi.org/10.1016/j.neuron.2014.04.023>

SUMMARY

An important strategy for efficient neural coding is to match the range of cellular responses to the distribution of relevant input signals. However, the structure and relevance of sensory signals depend on behavioral state. Here, we show that behavior modifies neural activity at the earliest stages of fly vision. We describe a class of wide-field neurons that provide feedback to the most peripheral layer of the *Drosophila* visual system, the lamina. Using *in vivo* patch-clamp electrophysiology, we found that lamina wide-field neurons respond to low-frequency luminance fluctuations. Recordings in flying flies revealed that the gain and frequency tuning of wide-field neurons change during flight, and that these effects are mimicked by the neuromodulator octopamine. Genetically silencing wide-field neurons increased behavioral responses to slow-motion stimuli. Together, these findings identify a cell type that is gated by behavior to enhance neural coding by subtracting low-frequency signals from the inputs to motion detection circuits.

INTRODUCTION

Vision must operate over an enormous range of natural conditions, from bright, open vistas to dingy, cluttered corners. Because natural scenes are dominated by low spatiotemporal frequencies (Laughlin, 1981), an efficient coding strategy is to suppress neural responses to low frequencies (Srinivasan et al., 1982). This principle, an example of predictive coding (Srinivasan et al., 1982), suggests that some neurons serve to reduce redundant visual features (Barlow, 1961), and thereby promote the encoding of important visual features by downstream circuits. One challenge for the predictive coding framework is that the statistics of visual scenes are subject to change. For example, the spectral distribution of natural scenes shifts toward higher frequencies when an animal is moving. Therefore, it might be useful for neurons that implement predictive coding to adapt their encoding properties based on the animal's behavioral state. Here, we describe a class of wide-field feedback neurons in the *Drosophila* visual system that provides low-frequency suppressive feedback signals at the inputs to motion detection

circuits, and whose tuning properties are modulated by the fly's behavioral state.

The fly optic lobes are organized into retinotopic columns, each corresponding to a small region of visual space (~5° diameter; Heisenberg and Wolf, 1984). In the lamina, the layer of neurons in the fly visual system after the photoreceptors (Figure 1A), each column, or "cartridge," contains processes of both columnar and multicolumnar neuron classes (Fischbach and Dittrich, 1989). Three of the columnar neurons, the lamina monopolar cells (LMCs) L1, L2, and L3, and the multicolumnar amacrine cells, receive direct input from the photoreceptors (Meinertzhagen and O'Neil, 1991; Rivera-Alba et al., 2011). L1 and L2 are required for motion detection (Clark et al., 2011; Joesch et al., 2010; Rister et al., 2007; Tuthill et al., 2013) and have been physiologically characterized in larger flies (Laughlin and Hardie, 1978) and *Drosophila* (Clark et al., 2011; Reiff et al., 2010; Zheng et al., 2006). Aside from the LMCs, however, the electrophysiological properties of other lamina neurons are not well understood.

Several synapses downstream of the lamina, a network of large tangential neurons in the lobula plate integrate local motion signals from across the fly's visual field (Borst et al., 2010). The response gain of these lobula plate tangential cells (LPTCs) increases during walking (Chiappe et al., 2010) and flight (Jung et al., 2011; Maimon et al., 2010; Suver et al., 2012), which may facilitate processing of higher image speeds during locomotion. Increased gain in LPTCs is triggered by release of the neuromodulator octopamine (Suver et al., 2012)—the invertebrate analog of vertebrate adrenergic transmitters such as adrenaline and norepinephrine (Farooqui, 2007). Although neurons that release octopamine in the lobula and medulla have been identified (Busch et al., 2009), the sites and mechanisms of octopamine neuromodulation are less clear. In this study, we show that octopamine-mediated behavioral state modulation extends to the most peripheral circuits of the fly visual system in the lamina.

RESULTS

During a screen of a collection of GAL4 lines (Jenett et al., 2012; Pfeiffer et al., 2008) for drivers with lamina expression (Tuthill et al., 2013), we identified a class of multicolumnar neurons in the *Drosophila* lamina that we call lamina wide-field 2 (abbreviated Lawf2; Figures 1A and 1B). This neuron type had not been described in classic Golgi surveys (Fischbach and Dittrich, 1989), but was recently observed in another study (Hasegawa

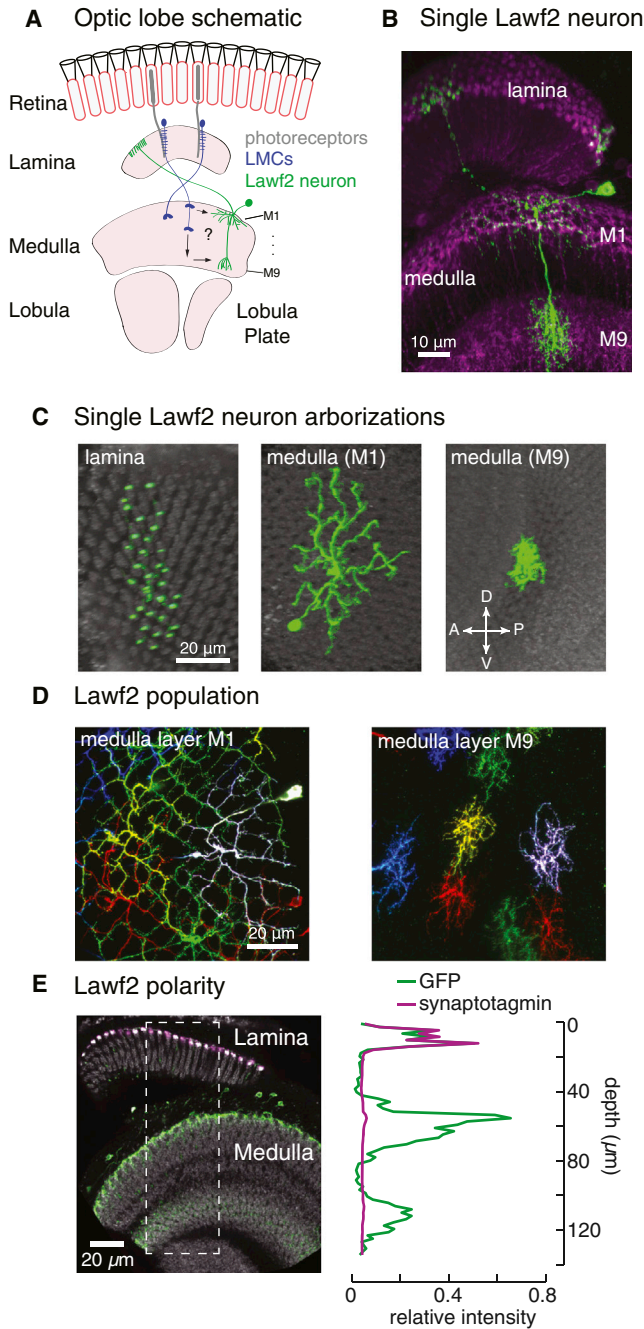


Figure 1. Anatomy of Lamina Wide-Field Neurons: Lawf2

(A) In the lamina, photoreceptor axons synapse on to L1, L2, and L3 neurons (example L1 and L3 neurons are illustrated). Wide-field neurons receive unknown inputs in the medulla and send an axon back into the lamina. (B) Stochastic single cell labeling of an individual wide-field neuron (green) with a membrane-targeted green fluorescent protein (GFP; see [Supplemental Experimental Procedures](#) for details). The entire pattern of the GAL4 driver used (R11D03) was labeled with mCD8 RFP (magenta). Markers were depicted using antibody staining with anti-GFP and anti-mCD8 antibodies, respectively. Image is a maximum intensity projection of a confocal substack. (C) Transverse sections of the arbors of an individual wide-field neuron show spread within specific layers. Images are substack projections of reoriented confocal stacks.

[et al., 2011](#)). Lawf2 is easily differentiated from another class of wide-field neurons (Lawf1; [Fischbach and Dittrich, 1989](#)), based on their distinct arborization patterns and physiological response properties ([Figures S1A–S1E](#) available online). There are ~140 Lawf2 neurons per optic lobe, and each lamina cartridge is innervated by ~5 Lawf2 cells (see [Supplemental Experimental Procedures](#) for details). Lawf2 branches in medulla layer M1 are large and overlapping (~120 retinal cartridges), and in M8–M10, they are smaller (~17 cartridges) and show less overlap ([Figures 1C and 1D](#)). Each Lawf2 neuron also sends a process into the lamina ([Figures 1B and 1C](#)), which innervates ~28 cartridges and is skewed along the dorsal-ventral axis ([Figure 1B](#); see [Supplemental Experimental Procedures](#) for detailed quantification). Expression of an epitope-tagged presynaptic marker, synaptotagmin ([Zhang et al., 2002](#)), in Lawf2 neurons revealed putative presynaptic sites in the lamina, but not the medulla ([Figure 1E](#)). In contrast, we found that Lawf1 has presynaptic sites in both the lamina and medulla ([Figure S1C](#)), consistent with recently published electron microscopic data ([Takemura et al., 2013](#)). We also found that expression of choline acetyltransferase ([Kolodziejczyk et al., 2008](#)) in the distal lamina overlaps with the bouton-like presynaptic terminals of Lawf2 ([Figure S1F](#)). Overall, these data indicate that Lawf2 neurons provide cholinergic feedback from the medulla to the lamina and are uniquely positioned to modulate signal encoding at the input to the motion detection pathway.

To characterize the physiological properties of Lawf2 neurons (hereafter referred to as “wide-field neurons”), we used in vivo targeted whole-cell patch-clamp electrophysiology ([Figure 2A](#)). In response to full-field luminance fluctuations, wide-field neurons depolarized after light onset and fired small numbers of spikes ([Figure 2B](#)). Two prominent features of wide-field neuron responses were that spike rates adapted across successive stimulus cycles, and that the time delay from light onset to the first spike was surprisingly long (>50 ms; [Figure S3B](#)). This response latency is longer than that of LPTCs (~30 ms; [Warzecha and Egelhaaf, 2000](#)) and should limit the ability of wide-field neurons to encode fast luminance fluctuations. Consistent with this, we found that wide-field neurons responded more strongly to low-frequency flicker ([Figure 2C](#)); faster flicker elicited only a transient spiking response ([Figure 2B](#), bottom). As expected from their morphology, wide-field neuron receptive fields were large (>30 retinotopic columns; [Figure 2D](#) and [Figure S2](#)), and cells responded most strongly to full-field light flashes ([Figure 2E](#)). Wide-field neurons were not selective for any particular direction of motion, but did respond to the luminance fluctuations present in motion stimuli ([Figures 2F and 2G](#)). Among all stimuli we explored, maximal responses were consistently

(D) Multicolor stochastic labeling of a subset of the population of wide-field neurons illustrates the different coverage in medulla layers M1 (~22-fold coverage) and M9 (~3-fold coverage).

(E) Localization of a presynaptic marker indicates that Lawf2 neurons provide feedback from the medulla to the lamina. Shown at left is the distribution of a FLAG-epitope-tagged membrane targeted GFP (green) and an HA-tagged presynaptic marker (synaptotagmin-HA) in Lawf2 neurons (magenta); nc82, a neuropil marker, is shown in gray. A Lawf2 specific split-GAL4 driver (R11D03AD; R19C10DBD) was used for marker expression. Quantification of GFP and synaptotagmin intensity within the outlined region is shown at right.

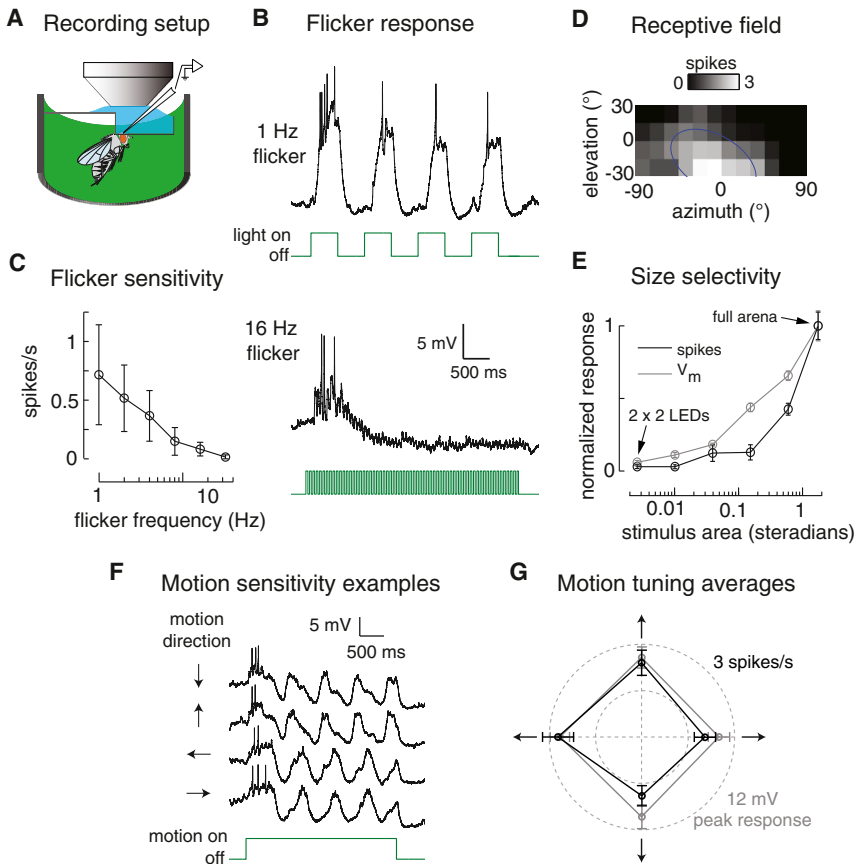


Figure 2. Wide-Field Neurons Integrate Luminance Changes in Space and Time, but Are Not Directionally Selective

(A) Schematic of the recording setup. The head of the fly is fixed, while patch clamp recordings are visually targeted to GFP-labeled wide-field neuron cell bodies. The eye is stimulated with a green LED arena.

(B) Example traces of a wide-field neuron in response to full-field flicker at two frequencies. When the flicker is slow, the cell spikes on each stimulus cycle; at higher frequencies, the cell spikes only at stimulus onset and not on subsequent cycles.

(C) Mean (\pm SEM) spike rates of wide-field neurons across a range of flicker frequencies. Wide-field neurons respond more strongly to low-frequency flicker stimuli ($p < 0.001$, one-way ANOVA, $n = 11$ cells). Flicker stimuli were full-field and maximum contrast, and spike rates were calculated across the last 3 s of the 4 s stimulus period.

(D) Wide-field neurons integrate luminance signals from large regions of the fly's visual field. Shown is an example receptive field, determined by flashing a $30^\circ \times 30^\circ$ bright square at 33 overlapping locations in the arena, and calculating the mean spike rate at each point.

(E) Mean (\pm SEM) spike rates and membrane potential depolarizations evoked by light stimuli of increasing area, demonstrating that wide-field neurons respond maximally to full-field light stimuli. For purposes of visual comparison, spike rates and membrane depolarizations were normalized to the maximum response for each cell. All stimuli were centered on the peak of the receptive field ($n = 10$ cells), and $5 \mu\text{M}$ octopamine was included in the bath to increase response amplitudes.

(F) Example traces of a wide-field neuron response to motion stimuli moving along the four cardinal axes of the eye. The stimuli consisted of $30^\circ \times 30^\circ$ alternating bright and dark blocks that moved at $45^\circ/\text{s}$ in the indicated direction (corresponding to a temporal frequency of 1.5 Hz). The periodic fluctuations in these responses are due to the fluctuations present in the motion stimuli (and occur at 1.5 Hz, precisely locked to the temporal frequency of the motion stimulus).

(G) Mean (\pm SEM) responses to visual motion stimuli ($n = 5$ cells). Neither spike rates nor peak subthreshold responses were significantly different for any particular direction of motion (one-way ANOVA), indicating that wide-field neurons are not directionally selective. Spike rates were calculated across the entire stimulus period (3 s), and maximum peak-to-peak responses were computed from the max-min V_m of each trial after filtering out spikes. Direction selectivity was also not observed in the presence of $5 \mu\text{M}$ octopamine ($n = 2$ cells, data not shown).

obtained with full-field flicker, and so we used this as the stimulus to further probe the response properties of wide-field neurons. Together, these data demonstrate that wide-field neurons have large receptive fields and signal slow luminance changes, but do not exhibit motion selectivity.

Previous studies of LPTC neurons in the lobula plate, a region several synapses downstream of the lamina, have found that visual response properties are modulated by behavior (Chiappe et al., 2010; Jung et al., 2011; Maimon et al., 2010; Suver et al., 2012). To test whether peripheral circuits of the lamina and medulla are also subject to behavioral state-dependent modulation, we performed whole-cell recordings of wide-field neurons during flight (Figure 3A). When the fly was flying, brief light flashes evoked higher spike rates (Figure 3B) and decreased the latency of the first stimulus-evoked spike (Figure 3C). Bath application of $5 \mu\text{M}$ octopamine mimicked the effects of flight (Figure 3A), suggesting that wide-field neuron activity is altered due to octopamine release during flight.

Due to the technical difficulty of achieving stable recordings in flying flies, we used bath application of octopamine in restrained flies to investigate behavioral state modulation of wide-field neurons in greater detail (Figures 3D–3G). We found that octopamine increased both spiking and subthreshold responses to light stimuli, and decreased spike latency (Figure 3D and Figure S3). Octopamine also dramatically altered the effects of dark adaptation on wide-field neuron activity. Neurons fired more spikes following extended periods of dark adaptation, and octopamine amplified the effects of adaptation (Figures 3F and 3G). Finally, octopamine increased depolarizing responses to light offset (Figure 3A and Figures S3D and S3E).

Because octopamine altered the response latency and excitability of wide-field neurons, we hypothesized that it could also affect their frequency sensitivity. To test this, we measured responses to full-field luminance flicker (Figure 4A). Under control conditions, wide-field neurons responded maximally to low-frequency flicker patterns (1–2 Hz), but when octopamine was

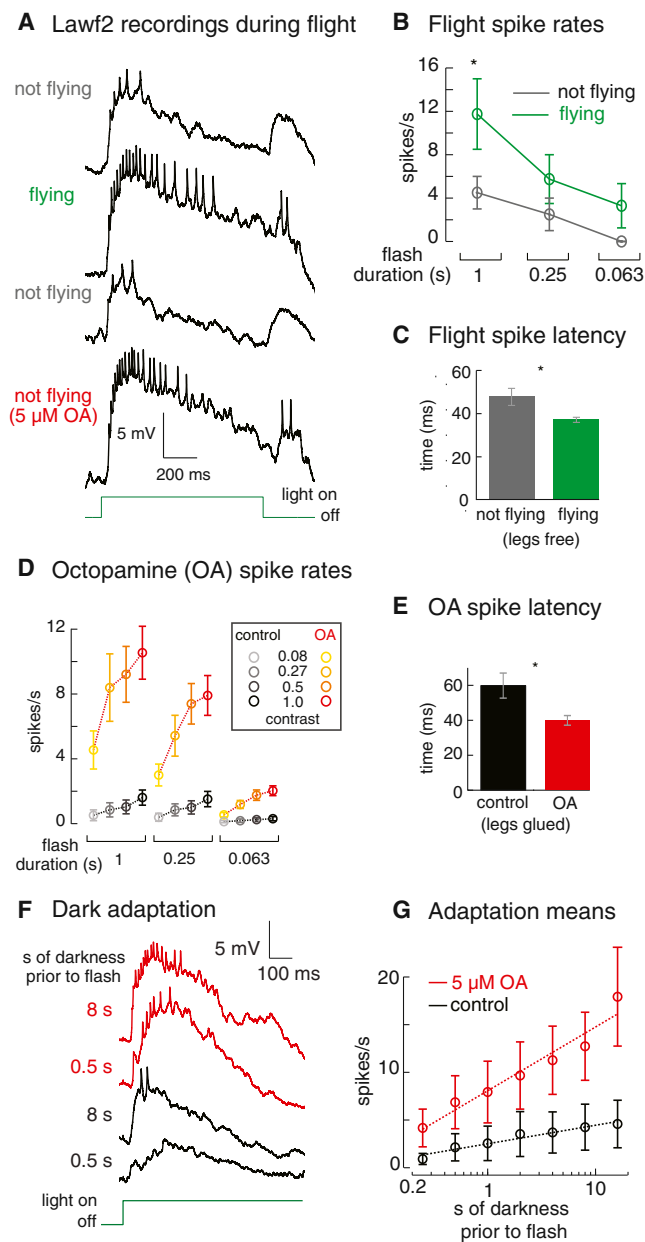


Figure 3. Flight Behavior Dramatically Enhances Wide-Field Neuron Activity

(A) Example wide-field neuron responses to a 1 s light flash before, during, and after flight. Application of the neuromodulator octopamine (OA; 5 μ M) mimicked the effects of flight.

(B) Wide-field neuron spike rates in response to light flashes increase during flight as compared to nonflying conditions (mean \pm SEM, * p < 0.05, paired t tests, n = 4 cells). The maximum stimulus contrast was used.

(C) Flight behavior decreases the latency to the first spike (mean \pm SEM) following a 1 s light flash (* p < 0.05, t test, n = 4 cells).

(D) Octopamine significantly increases spike rates (mean \pm SEM) across contrast conditions and flash durations (p < 0.001, one-way ANOVA, n = 11 cells).

(E) Octopamine decreases spike latency (mean \pm SEM) following a 1 s light flash (* p < 0.05, paired t test, n = 8 cells).

(F) Examples of flash responses following different periods of dark adaptation, with (red) and without (black) octopamine.

present, spike rates increased dramatically at all frequencies (Figure 4B). In addition to this increase in overall gain, the peak of the frequency sensitivity tuning curve for both spiking and subthreshold responses shifted toward higher frequencies (Figure 4B and Figure S4). We also observed that subthreshold responses decreased at the lowest frequency tested (Figure 4B), which appears to result from the emergence of responses to light offset when octopamine is present (Figure S4A). Overall, these data indicate that octopamine release during flight boosts wide-field neuron activity and enhances signaling of higher frequencies.

Octopamine acts through G protein-coupled receptors to exert diverse neuromodulatory effects throughout the insect nervous system (Farooqui, 2007). The axonal projections of some octopamine neurons overlap with the dendritic arbors of wide-field neurons in the medulla (Busch et al., 2009), raising the possibility that octopamine directly modulates wide-field neuron activity. To test this, we injected square current pulses to measure the effect of octopamine on wide-field neuron spiking (Figure 4C). Current injection evoked higher spike rates when octopamine was present (Figure 4D, top panel), and the latency to the first spike in response to current injection decreased (19.2 ± 1.8 versus 10.2 ± 0.8 ms; p < 0.001, n = 14 cells; current step of 50 pA). Although octopamine did not affect the input resistance measured at the cell soma (control, 1.07 ± 0.08 G Ω ; octopamine, 1.02 ± 0.06 G Ω ; p = 0.63, n = 14 cells), the resting potential depolarized slightly (-61.0 versus -57.6 mV, p = 0.05, n = 14 cells). These data suggest that the octopamine-mediated changes in light-evoked activity may result from direct neuromodulation of wide-field neurons. However, changes in intrinsic properties could also result through modulation of circuit elements that provide synaptic input to wide-field neurons. To distinguish between these two hypotheses, we used CdCl₂, which blocks voltage-dependent calcium channels and therefore eliminates synaptic transmission (Figure 4C). Although Cd²⁺ effectively abolished all light-evoked responses (data not shown), the increase in excitability due to octopamine persisted (Figure 4D, bottom). This result indicates that octopamine directly increases wide-field neuron excitability, and suggests that the behavioral state-dependent effects on light-evoked activity may be at least partially due to targeted neuromodulation of wide-field neurons.

Our anatomy and electrophysiology data suggest that wide-field neurons are well positioned to modify the activity of lamina neurons that provide input to motion detection circuits. In a previous survey of lamina neuron function, we observed that genetically silencing wide-field neurons had only subtle effects on behavioral responses to visual motion stimuli (Tuthill et al., 2013). Given that wide-field neurons encode low-frequency luminance fluctuations (Figure 2), we decided to further investigate how wide-field neurons shape fly responses to large, slow-motion stimuli.

As in the previous study (Tuthill et al., 2013), we used the Split-GAL4 method to silence wide-field neurons (Figure 5A and Figure S5) by expression of the Kir2.1 potassium channel (Baines

(G) Octopamine increases flash-evoked spike rates (mean \pm SEM, p < 0.001, ANOVA, n = 5 cells; slope of red line = 2.01, R^2 = 0.94; black line = 0.58, R^2 = 0.95).

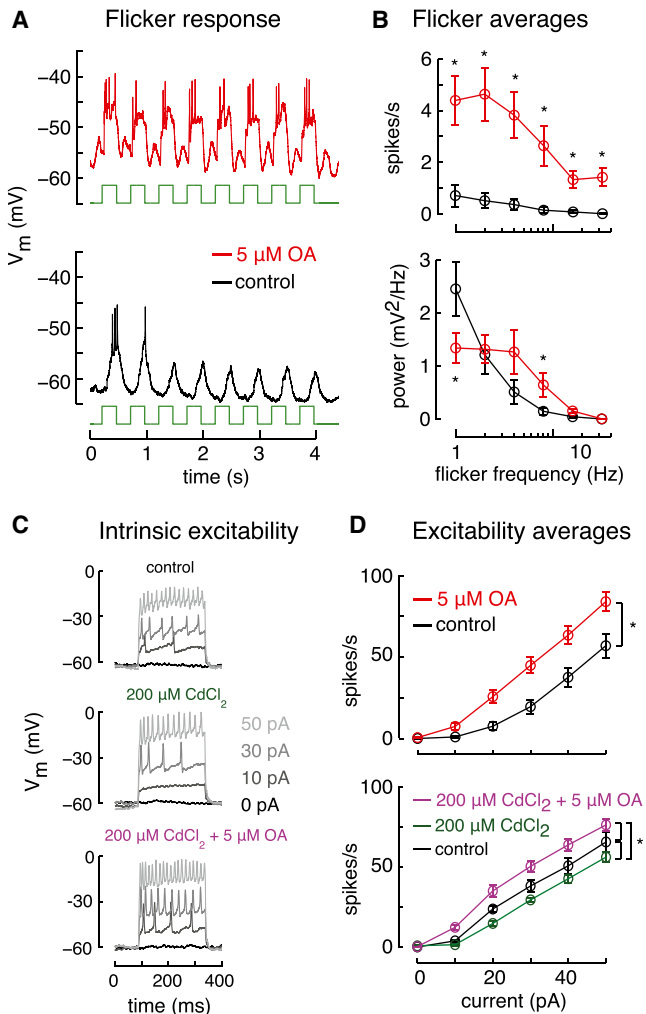


Figure 4. Octopamine Enhances Sensitivity to High-Frequency Luminance Fluctuations and Increases Wide-Field Neuron Excitability

(A) Example traces of a wide-field neuron in response to a 2 Hz full-field flicker stimulus. OA, octopamine.

(B) Octopamine increases spike rates (top) and power of membrane potential fluctuations at the flicker frequency (bottom; mean \pm SEM, * p < 0.05, paired t tests, n = 10 cells). See Figure S4 for power spectra and spike rates across contrast conditions.

(C) Octopamine increases wide-field neuron excitability. Shown are example traces of a wide-field neuron to sequential current steps in normal saline (top), after blocking synaptic transmission with Cd^{2+} (middle), and in the presence of both octopamine and Cd^{2+} (bottom). These example data correspond to (D, bottom).

(D) Average effects of octopamine on wide-field neuron spike rates (mean \pm SEM). (Top) Wide-field neurons fired significantly more spikes with 5 μM octopamine in the bath (repeated-measures ANOVA; p < 0.01 for current, p = 0.01 for OA, n = 14 cells). (Bottom) Octopamine increased spike rates even when synaptic inputs to wide-field neurons were blocked with Cd^{2+} . Octopamine application increased spike rates over both control (p < 0.01 for current; p < 0.05 for OA, n = 4 cells) and CdCl_2 conditions (p < 0.01 for current; p < 0.01 for OA, n = 4). Application of CdCl_2 alone also decreased current-evoked spike rates (repeated-measures ANOVA; p < 0.01 for current; p < 0.05 for CdCl_2 n = 4 cells). There was no significant difference in the resting membrane potential, input resistance, or spontaneous activity among the three conditions (paired t tests).

et al., 2001) and quantified fly behavioral responses to visual motion stimuli. We measured visual behavior in tethered flying flies positioned within a cylindrical LED arena (Figure 5B; see Supplemental Experimental Procedures or Reiser and Dickinson, 2008 for details). In the flight arena, we used an optical wingbeat analyzer (Götz, 1987) to measure the difference between the left and right wingbeat amplitude (ΔWBA), a metric that is proportional to yaw steering torque (Tammero et al., 2004). We compared the flight steering responses of two experimental Split-GAL4 lines crossed to UAS-Kir2.1 to the behavioral responses of two control lines (each an individual Split-GAL4 half also crossed to UAS-Kir2.1). We then used a conservative statistical criterion, where for each stimulus condition, we report as significant only those cases where both of the Split-GAL4 lines are individually, significantly different from the responses of the control lines, while applying false discovery rate correction (see Supplemental Experimental Procedures for details).

We found that silencing wide-field neurons increased flight turning responses to very low-frequency motion stimuli, while responses to higher frequency motion were unaffected (Figures 5C, 5D, and S5B). This result is consistent with the hypothesis that wide-field neuron feedback suppresses low frequencies within premotion lamina circuits, and that removing this suppressive feedback signal increases sensitivity to low frequencies.

To further investigate this behavioral phenotype, we used a psychophysical technique called motion nulling (Figure 5E; Cavanagh and Anstis, 1991; Smear et al., 2007; Tuthill et al., 2013). When presented with conflicting motion stimuli moving at different speeds, flies will typically turn in the direction of the faster stimulus, even if it has lower contrast. Using this technique, we measured fly contrast sensitivity as a function of temporal frequency by varying the velocity and contrast of one motion stimulus across trials, while the parameters of the other motion stimulus remained constant. Silencing wide-field neurons increased the tendency of flies to follow slow-motion stimuli (Figure 5F). In other words, when presented with a very slow high contrast stimulus, and a faster low contrast stimulus, flies with silenced wide-field neurons steered in the direction of the slower stimulus (Figures S5C and S5D). This effect was remarkably specific to slow stimulus speeds (Figure 5F), again supporting the hypothesis that wide-field neuron feedback suppresses low frequency signals within pre-motion pathways in the lamina. Importantly, the motion nulling experiment provides a relative measure of speed sensitivity, indicating that the observed shift in visual sensitivity does not result from a saturation of steering responses or a general impairment of flight behavior. In addition, flies with silenced wide-field neurons showed normal responses to many other visual stimuli (Tuthill et al., 2013).

To validate the feedback suppression model, we simulated the output of lamina monopolar cells (LMCs) with and without wide-field neuron feedback to natural luminance time series (Figure 6A; van Hateren, 1997). Subtractive feedback from wide-field neurons flattened the power spectrum of model LMC responses at low frequencies (<10 Hz; Figure 6B). This flattened response distribution is highly consistent with recordings from blowfly LMCs (Laughlin, 1981; van Hateren, 1997), and is indicative of an efficient coding strategy to maximize information transmission (Laughlin, 1981). We then used the same lamina model to

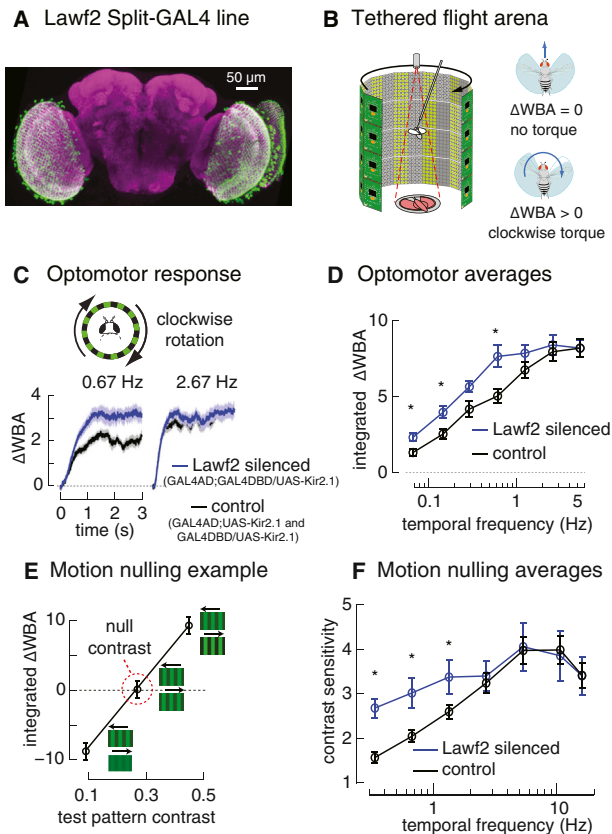


Figure 5. Silencing Wide-Field Neurons Increases Flight Steering Responses to Slow Visual Motion

(A) One of two Split-GAL4 lines used for behavioral experiments (R11D03AD; R19C10DBD). The GAL4 expression pattern was visualized by anti-GFP antibody staining (in green; neuropil in magenta). For behavioral experiments, we compare the responses of two experimental Split-GAL4 lines crossed to UAS-Kir2.1 to the behavioral responses of two control lines (each an individual Split-GAL4 half also crossed to UAS-Kir2.1).

(B) Schematic of the visual display arena used for flight behavior experiments. Individual wingstrokes of tethered flies are tracked by an optical detector. The difference between the left and right wingbeat amplitude (Δ WBA) is recorded as the turning response because it is proportional to the steering torque generated by the fly.

(C) Silencing wide-field neurons with Kir2.1 expression increases fly responses to slow-motion stimuli. Each trace shows the mean turning responses of flies to the rotation of a striped grating pattern (90° spatial period; temporal frequency noted; maximum pattern contrast).

(D) Integrated turning responses (mean \pm SEM, $n > 12$ flies per genotype, $*p < 0.05$). See Figure S5 for the complete data set and the Supplemental Experimental Procedures for details of the statistical analysis.

(E) Motion nulling stimuli consist of two superimposed square-wave gratings ($\lambda = 45^\circ$): a constant reference stimulus, and a test stimulus whose contrast is varied across trials. In this example, flies follow the reference stimulus (Δ WBA < 0) when the test contrast is low; at high-test contrast, flies follow the test stimulus (Δ WBA > 0). The null contrast is the contrast of the test stimulus needed to cancel, or “null,” the reference stimulus for each speed of the test stimulus. Contrast sensitivity is defined as the inverse of the null contrast (Smear et al., 2007).

(F) Silencing wide-field neurons increases sensitivity to low stimulus velocities (mean \pm SEM; see Figure S5 for complete data set).

simulate the response of an array of elementary motion detectors (Hassenstein and Reichardt, 1956) to motion stimuli like those used in the flight behavior experiments (Figure 5D). Removing wide-field neuron feedback from the lamina model increased simulated responses to slow-motion stimuli (Figure 6C), consistent with the behavioral phenotype observed when silencing wide-field neurons (Figure 5D).

DISCUSSION

The survival of a fly depends critically on being able to detect subtle changes in the contrast and spatial position of objects in the environment. Flies perform such discriminations across diverse lighting conditions and visual environments. Consequently, visual neurons must be able to extract the most relevant signals from highly variable natural scenes.

The anatomy and physiology of wide-field neurons suggests that their role is to implement low-frequency suppression in the fly lamina. Wide-field feedback may increase the coding efficiency of lamina neurons by subtracting redundant, low-frequency signals. This hypothesis is supported by our finding that silencing wide-field neurons increased flight steering responses to low-frequency motion stimuli (Figure 5). The functional role of lamina wide-field neurons may be similar to some amacrine cells in the vertebrate retina, which provide wide-field feedback onto bipolar cells in the inner plexiform layer (Masland, 2012).

Structure of Potential Feedback Circuits

The basic morphology of wide-field neurons, combined with labeling of presynaptic sites with synaptotagmin (Figure 1) and previous electron microscopy data (Rivera-Alba et al., 2011), indicate that wide-field neurons provide feedback from the medulla to the lamina. Although the presynaptic inputs to wide-field neurons are not known, the long response latency (Figure S3) suggests that there may be several synapses between the photoreceptors and wide-field neurons. The likely postsynaptic targets of wide-field neurons can be inferred from an examination of wide-field neuron processes identified within an individual lamina column reconstructed using electron microscopy. It is likely that wide-field neurons form synapses on most cell types in the lamina, with particularly high concentrations on the lamina intrinsic amacrine cells and L3 (Rivera-Alba et al., 2011). The LMCs, including L3, are sign-inverted with respect to the photoreceptors—they hyperpolarize in response to luminance increases (Hardie and Weckström, 1990; Sillescu et al., 2013). Antibody staining suggests that wide-field neurons likely release acetylcholine (Figure S1F). Because acetylcholine depolarizes LMCs (Hardie, 1988), cholinergic inputs from wide-field neurons would therefore inhibit light-evoked hyperpolarization within the LMCs and serve as a suppressive feedback signal. Alternatively, feedback from wide-field neurons onto lamina intrinsic amacrine cells, which provide synaptic input to all of the columnar lamina neuron types (Rivera-Alba et al., 2011), could more broadly influence signals in the lamina. Interestingly, silencing L3 neurons specifically affects behavioral responses to slow-motion stimuli (Tuthill et al., 2013) and calcium imaging results indicate that L3 is primarily sensitive to light decrements and has long-lasting response kinetics compared to L1 and L2

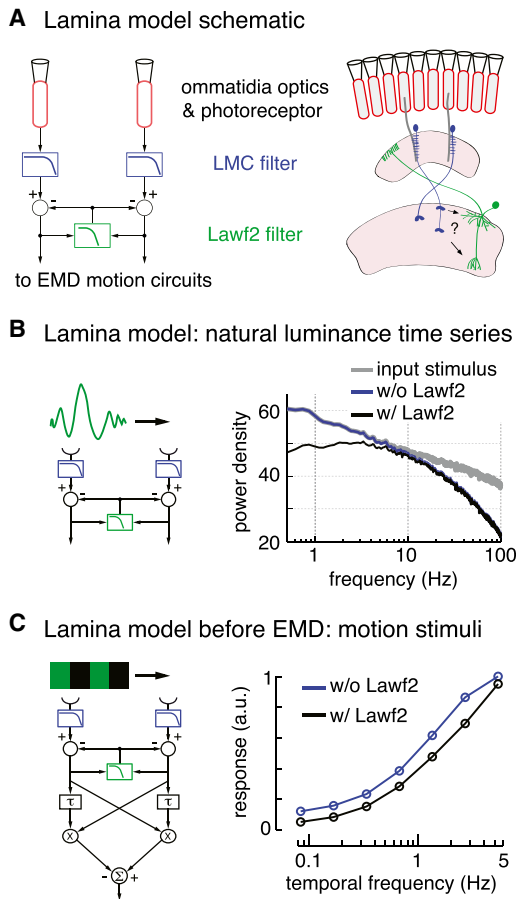


Figure 6. A Model for Lamina Processing with Wide-Field Neuron Feedback

(A) Peripheral preprocessing units (photoreceptors and LMCs) and wide-field neurons were modeled as low-pass filters with time constants of $\tau = 8$ ms and 24 ms, respectively. See [Supplemental Experimental Procedures](#) for details. In this model, the Lawf2 filter output is subtracted from the feed-forward signals.

(B) Power spectral density of model responses to 100 s of naturalistic luminance time series. The three curves represent the power spectral density of the input time series (gray), the output of a model with wide-field neuron feedback (black), and the output of a model without feedback (blue). Including wide-field neuron feedback flattens the response at frequencies < 10 Hz.

(C) Simulated responses of an array of Hassenstein-Reichardt elementary motion detectors (EMDs; model detailed in [Supplemental Experimental Procedures](#)) that are preceded by lamina processing units, with and without wide-field neuron feedback. The model was stimulated with the identical visual pattern used in the behavioral experiments in [Figure 5D](#). Silencing the wide-field neuron feedback in the simulation increased responses to slow-motion stimuli (< 5 Hz), in agreement with the behavioral silencing result.

(Silies et al., 2013). This raises the possibility that feedback from wide-field neurons contributes to the long response decay observed in L3. Direct measurement of the impact of wide-field neuron feedback on LMCs will be required to test this model.

Advantages of Predictive Feedback

Lateral suppression is known to exist within and between neighboring cartridges in the fly lamina (Laughlin and Hardie, 1978;

Srinivasan et al., 1982). However, correlations in natural scenes exist across spatial and temporal scales much larger than signals within individual lamina columns. The spectral power of natural images decreases according to a power law (e.g., $1/\text{frequency}$), such that natural scenes are dominated by low frequencies (van der Schaaf and van Hateren, 1996; van Hateren, 1997). Moving natural scenes are also dominated by low spatial and temporal frequencies (Dong and Atick, 1995). Wide-field feedback could serve to reduce redundancy in peripheral visual circuits through spatiotemporal predictive coding (Srinivasan et al., 1982). A simple model of wide-field neuron feedback (Figure 6) suggests that this feedback acts to filter low-frequency signals, increasing the relative sensitivity to higher frequencies that are less common in visual scenes, but more informative for flight behavior. Several unique features of wide-field neurons make them well suited to this purpose.

In comparison to the LMCs, which are the feed-forward output neurons of the lamina, wide-field neuron spatial receptive fields are large and response latencies are long (Figure 2). By averaging over large areas of space and long intervals in time, the feedback signal from wide-field neurons will be resistant to local noise fluctuations. The contrast sensitivity of wide-field neurons is also comparatively low—under resting conditions (i.e., not flying), neurons respond only weakly (< 1 spike/s) to contrasts under 10% (Figure 3D). This weak sensitivity should serve as another noise filter, but would not prevent wide-field neurons from responding under natural conditions because contrast distributions in natural scenes are typically high (Laughlin, 1981).

A third noise-reducing feature of wide-field neuron is the spiking nonlinearity (Figure 2B). The lamina wide-field neurons we describe here are the only identified class of neurons in the fly lamina that are known to fire spikes under natural conditions. A spike threshold provides a mechanism for signaling large luminance changes without responding to transient input fluctuations. In contrast, we found that the other class of lamina wide-field feedback neurons, Lawf1, is nonspiking (Figures S1A–S1E). Feedback from Lawf1 and Lawf2 may serve distinct functions, for example, by providing feedback signals with unique temporal or spatial properties, or by operating under different luminance conditions.

Finally, the frequency tuning of wide-field neurons depends on behavioral state (Figure 4). When they are walking or flying, flies encounter higher temporal frequencies due to self-motion. Wide-field feedback from the medulla provides a pathway by which behavioral state could tune the strength and temporal characteristics of signal suppression at the earliest stages of visual processing. This state-dependent modulation of visual coding may serve to stabilize behavioral reflexes under different visual conditions, or reduce energy consumption by altering the sensitivity of the motion pathway only in situations where it is necessary to respond to higher frequencies, such as flight.

Sources of Behavioral State Modulation

Our characterization of wide-field neurons suggests that behavioral state modulation affects neural coding in the lamina and that this modulation is due to the release of the neuromodulator octopamine. Both flight and octopamine application increased the amplitude of stimulus-evoked responses and decreased

spike latency (Figure 3). Three pieces of evidence suggest that octopamine directly modifies wide-field neuron activity. First, bath application of octopamine significantly increased spike rates evoked by current injection (Figure 4D) and slightly depolarized the resting membrane potential. The increase in spiking due to octopamine persisted even when synaptic inputs were blocked with Cd^{2+} (Figure 4C), indicating that octopamine is capable of directly modulating wide-field neuron excitability. Second, the axonal projections of some octopamine neurons (e.g., OA-AL-2i3) terminate in the same layers of the medulla that contain the dendritic arbors of wide-field neurons (Busch et al., 2009). Third, an ongoing quantitative study of nuclear gene expression (Henry et al., 2012) found that *Lawf2* and *Lawf1* neurons express high levels of the octopamine receptor OAMB (Han et al., 1998), as compared to the other ten lamina neuron classes (Fred Davis, Lee Henry, and Sean Eddy, personal communication). Overall, these data suggest that at least some of the behavioral state changes we observed in wide-field neurons may be due to direct octopaminergic neuromodulation, although there are likely to be additional effects that arise elsewhere in the circuit.

A series of recent studies have demonstrated that active behavior modulates the coding properties of motion-sensitive LPTC neurons in the fly lobula plate (Chiappe et al., 2010; Jung et al., 2011; Maimon et al., 2010; Suver et al., 2012) and that this modulation may be due to release of the neuromodulator octopamine (Jung et al., 2011; Suver et al., 2012). It is not known whether the effects of octopamine on lobula plate neurons are due to direct neuromodulation or act through modulation of upstream neurons in the medulla, although recent experiments suggest a presynaptic origin (de Haan et al., 2012). Wide-field neurons may contribute to the behavioral state modulation of LPTCs, but they are not likely to be the sole locus of such neuromodulation, given the dense innervation of the lobula and medulla by octopamine neurons (Busch et al., 2009). Overall, our results demonstrate that state-dependent changes in speed sensitivity are not limited to the downstream LPTC neurons and likely reflect coordinated tuning along the motion detection pathway. Using feedback to shift the sensitivity of peripheral circuits during behavior is a powerful strategy for efficient neural coding and may be implemented in other sensory modalities and brain regions.

EXPERIMENTAL PROCEDURES

Procedures are briefly summarized below. Further details are provided in the [Supplemental Experimental Procedures](#).

Anatomy

Indirect immunofluorescence of fly brains was performed as previously described (Tuthill et al., 2013). A “flip-out”-based approach (Struhl and Basler, 1993) was used for stochastic single cell labeling with one or more colors. Additional images of single wide-field neurons were obtained by screening the optic lobe data set of the *Janelia Fly Light Single Neuron Project*.

Electrophysiology

In vivo whole-cell current-clamp recordings were made from green fluorescent protein-labeled wide-field neuron cell bodies. The fly was mounted in a custom steel holder, and a small piece of the cuticle was manually removed to expose the brain. The brain was continuously bathed in oxygenated saline. Visual

stimuli were delivered to the fly eye with a half-cylindrical green LED panel array (Reiser and Dickinson, 2008).

Behavior

Two Split-GAL4 lines were used to target wide-field neurons: R11D03AD;R19C10DBD and R11D03AD;R61H02DBD (Tuthill et al., 2013). Neurons were silenced by expression of the Kir2.1 potassium channel (Baines et al., 2001). Female *Drosophila*, 3–5 days old, were glued to a tungsten pin and positioned in a virtual reality flight arena consisting of green LED panels (Reiser and Dickinson, 2008). Wingbeat amplitudes were measured and analyzed as previously described (Tuthill et al., 2013).

SUPPLEMENTAL INFORMATION

Supplemental Information includes Supplemental Experimental Procedures and five figures and can be found with this article online at <http://dx.doi.org/10.1016/j.neuron.2014.04.023>.

ACKNOWLEDGMENTS

We thank Mehmet Fişek, Vivek Jayaraman, Eugenia Chiappe, Gaby Maimon, and Gabe Murphy for help with developing the electrophysiology preparation; Jinyang Liu and Magnus Karlsson for assistance with the visual display system; Parvez Ahammad for help with signal processing routines; Barret Pfeiffer for design and construction of genetic constructs; the *Janelia Fly Light Project Team* for some confocal images; *Janelia Scientific Computing for Image Processing Software*; and members of the Reiser, Jayaraman, and Card labs at JFRC for technical assistance and use of equipment. We thank Rachel Wilson for providing space and equipment for the experiments in Figure 4C. Finally, we thank Rachel Wilson, Gabe Murphy, Vivek Jayaraman, Brett Mensh, and Nelson Spruston for comments on the manuscript. This project was supported by HHMI.

Accepted: March 28, 2014

Published: May 21, 2014

REFERENCES

- Baines, R.A., Uhler, J.P., Thompson, A., Sweeney, S.T., and Bate, M. (2001). Altered electrical properties in *Drosophila* neurons developing without synaptic transmission. *J. Neurosci.* *21*, 1523–1531.
- Bartlow, H.B. (1961). The coding of sensory messages. In *Current problems in animal behavior*, W.H. Thorpe and G.J. Mitchison, eds. (Cambridge: Cambridge University Press).
- Borst, A., Haag, J., and Reiff, D.F. (2010). Fly motion vision. *Annu. Rev. Neurosci.* *33*, 49–70.
- Busch, S., Selcho, M., Ito, K., and Tanimoto, H. (2009). A map of octopaminergic neurons in the *Drosophila* brain. *J. Comp. Neurol.* *513*, 643–667.
- Cavanagh, P., and Anstis, S. (1991). The contribution of color to motion in normal and color-deficient observers. *Vision Res.* *31*, 2109–2148.
- Chiappe, M.E., Seelig, J.D., Reiser, M.B., and Jayaraman, V. (2010). Walking modulates speed sensitivity in *Drosophila* motion vision. *Curr. Biol.* *20*, 1470–1475.
- Clark, D.A., Bursztyn, L., Horowitz, M.A., Schnitzer, M.J., and Clandinin, T.R. (2011). Defining the computational structure of the motion detector in *Drosophila*. *Neuron* *70*, 1165–1177.
- de Haan, R., Lee, Y.J., and Nordstrom, K. (2012). Octopaminergic modulation of contrast sensitivity. *Front. Integr. Neurosci.* *6*, 55.
- Dong, D.W., and Atick, J.J. (1995). Statistics of natural time-varying images. *Network* *6*, 345–358.
- Farooqui, T. (2007). Octopamine-mediated neuromodulation of insect senses. *Neurochem. Res.* *32*, 1511–1529.
- Fischbach, K.F., and Dittrich, A.P. (1989). The optic lobe of *Drosophila melanogaster*. I. A Golgi analysis of wild-type structure. *Cell Tissue Res.* *258*, 441–475.

- Götz, K.G. (1987). Course-control, metabolism and wing interference during ultralong tethered flight in *Drosophila melanogaster*. *J. Exp. Biol.* *128*, 35–46.
- Han, K.A., Millar, N.S., and Davis, R.L. (1998). A novel octopamine receptor with preferential expression in *Drosophila* mushroom bodies. *J. Neurosci.* *18*, 3650–3658.
- Hardie, R.C. (1988). Effects of antagonists on putative histamine-receptors in the 1st visual neuropil of the housefly (*Musca Domestica*). *J. Exp. Biol.* *138*, 221–241.
- Hardie, R.C., and Weckström, M. (1990). Three classes of potassium channels in large monopolar cells of the blowfly *Calliphora vicina*. *J. Comp. Physiol. A Neuroethol. Sens. Neural Behav. Physiol.* *167*, 723–736.
- Hasegawa, E., Kitada, Y., Kaido, M., Takayama, R., Awasaki, T., Tabata, T., and Sato, M. (2011). Concentric zones, cell migration and neuronal circuits in the *Drosophila* visual center. *Development* *138*, 983–993.
- Hassenstein, V.B., and Reichardt, W. (1956). Systemtheoretische analyse der zeit-, reihenfolgen- und vorzeichenbewertung bei der bewegungsperzeption des rüsselkäfers *Chlorophanus*. *Z. Naturforsch.* *11*, 513–524.
- Heisenberg, M., and Wolf, R. (1984). Vision in *Drosophila*: Genetics of Microbehavior. (Berlin: Springer-Verlag).
- Henry, G.L., Davis, F.P., Picard, S., and Eddy, S.R. (2012). Cell type-specific genomics of *Drosophila* neurons. *Nucleic Acids Res.* *40*, 9691–9704.
- Jenett, A., Rubin, G.M., Ngo, T.T., Shepherd, D., Murphy, C., Dionne, H., Pfeiffer, B.D., Cavallaro, A., Hall, D., Jeter, J., et al. (2012). A GAL4-driver line resource for *Drosophila* neurobiology. *Cell Rep.* *2*, 991–1001.
- Joesch, M., Schnell, B., Raghu, S.V., Reiff, D.F., and Borst, A. (2010). ON and OFF pathways in *Drosophila* motion vision. *Nature* *468*, 300–304.
- Jung, S.N., Borst, A., and Haag, J. (2011). Flight activity alters velocity tuning of fly motion-sensitive neurons. *J. Neurosci.* *31*, 9231–9237.
- Kolodziejczyk, A., Sun, X., Meinertzhagen, I.A., and Nässel, D.R. (2008). Glutamate, GABA and acetylcholine signaling components in the lamina of the *Drosophila* visual system. *PLoS ONE* *3*, e2110.
- Laughlin, S. (1981). A simple coding procedure enhances a neuron's information capacity. *Z. Naturforsch., C, Biosci.* *36*, 910–912.
- Laughlin, S.B., and Hardie, R.C. (1978). Common strategies for light adaptation in the peripheral visual systems of fly and dragonfly. *J. Comp. Physiol. A Neuroethol. Sens. Neural Behav. Physiol.* *128*, 319–340.
- Maimon, G., Straw, A.D., and Dickinson, M.H. (2010). Active flight increases the gain of visual motion processing in *Drosophila*. *Nat. Neurosci.* *13*, 393–399.
- Masland, R.H. (2012). The tasks of amacrine cells. *Vis. Neurosci.* *29*, 3–9.
- Meinertzhagen, I.A., and O'Neil, S.D. (1991). Synaptic organization of columnar elements in the lamina of the wild type in *Drosophila melanogaster*. *J. Comp. Neurol.* *305*, 232–263.
- Pfeiffer, B.D., Jenett, A., Hammonds, A.S., Ngo, T.T., Misra, S., Murphy, C., Scully, A., Carlson, J.W., Wan, K.H., Laverty, T.R., et al. (2008). Tools for neuroanatomy and neurogenetics in *Drosophila*. *Proc. Natl. Acad. Sci. USA* *105*, 9715–9720.
- Reiff, D.F., Plett, J., Mank, M., Griesbeck, O., and Borst, A. (2010). Visualizing retinotopic half-wave rectified input to the motion detection circuitry of *Drosophila*. *Nat. Neurosci.* *13*, 973–978.
- Reiser, M.B., and Dickinson, M.H. (2008). A modular display system for insect behavioral neuroscience. *J. Neurosci. Methods* *167*, 127–139.
- Rister, J., Pauls, D., Schnell, B., Ting, C.Y., Lee, C.H., Sinakevitch, I., Morante, J., Strausfeld, N.J., Ito, K., and Heisenberg, M. (2007). Dissection of the peripheral motion channel in the visual system of *Drosophila melanogaster*. *Neuron* *56*, 155–170.
- Rivera-Alba, M., Vitaladevuni, S.N., Mishchenko, Y., Lu, Z., Takemura, S.Y., Scheffer, L., Meinertzhagen, I.A., Chklovskii, D.B., and de Polavieja, G.G. (2011). Wiring economy and volume exclusion determine neuronal placement in the *Drosophila* brain. *Curr. Biol.* *21*, 2000–2005.
- Silies, M., Gohl, D.M., Fisher, Y.E., Freifeld, L., Clark, D.A., and Clandinin, T.R. (2013). Modular use of peripheral input channels tunes motion-detecting circuitry. *Neuron* *79*, 111–127.
- Smear, M.C., Tao, H.W., Staub, W., Orger, M.B., Gosse, N.J., Liu, Y., Takahashi, K., Poo, M.M., and Baier, H. (2007). Vesicular glutamate transport at a central synapse limits the acuity of visual perception in zebrafish. *Neuron* *53*, 65–77.
- Srinivasan, M.V., Laughlin, S.B., and Dubs, A. (1982). Predictive coding: a fresh view of inhibition in the retina. *Proc. R. Soc. Lond. B Biol. Sci.* *216*, 427–459.
- Struhl, G., and Basler, K. (1993). Organizing activity of wingless protein in *Drosophila*. *Cell* *72*, 527–540.
- Suver, M.P., Mamiya, A., and Dickinson, M.H. (2012). Octopamine neurons mediate flight-induced modulation of visual processing in *Drosophila*. *Curr. Biol.* *22*, 2294–2302.
- Takemura, S.Y., Bharioke, A., Lu, Z., Nern, A., Vitaladevuni, S., Rivlin, P.K., Katz, W.T., Olbris, D.J., Plaza, S.M., Winston, P., et al. (2013). A visual motion detection circuit suggested by *Drosophila* connectomics. *Nature* *500*, 175–181.
- Tammero, L.F., Frye, M.A., and Dickinson, M.H. (2004). Spatial organization of visuomotor reflexes in *Drosophila*. *J. Exp. Biol.* *207*, 113–122.
- Tuthill, J.C., Nern, A., Holtz, S.L., Rubin, G.M., and Reiser, M.B. (2013). Contributions of the 12 neuron classes in the fly lamina to motion vision. *Neuron* *79*, 128–140.
- van der Schaaf, A., and van Hateren, J.H. (1996). Modelling the power spectra of natural images: statistics and information. *Vision Res.* *36*, 2759–2770.
- van Hateren, J.H. (1997). Processing of natural time series of intensities by the visual system of the blowfly. *Vision Res.* *37*, 3407–3416.
- Warzecha, A., and Egelhaaf, M. (2000). Response latency of a motion-sensitive neuron in the fly visual system: dependence on stimulus parameters and physiological conditions. *Vision Res.* *40*, 2973–2983.
- Zhang, Y.Q., Rodesch, C.K., and Broadie, K. (2002). Living synaptic vesicle marker: synaptotagmin-GFP. *Genesis* *34*, 142–145.
- Zheng, L., de Polavieja, G.G., Wolfram, V., Asyali, M.H., Hardie, R.C., and Juusola, M. (2006). Feedback network controls photoreceptor output at the layer of first visual synapses in *Drosophila*. *J. Gen. Physiol.* *127*, 495–510.

Neuron, Volume 82

Supplemental Information

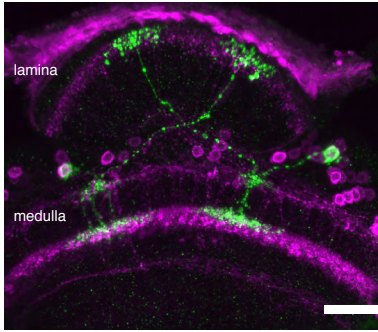
Wide-Field Feedback Neurons

Dynamically Tune Early Visual Processing

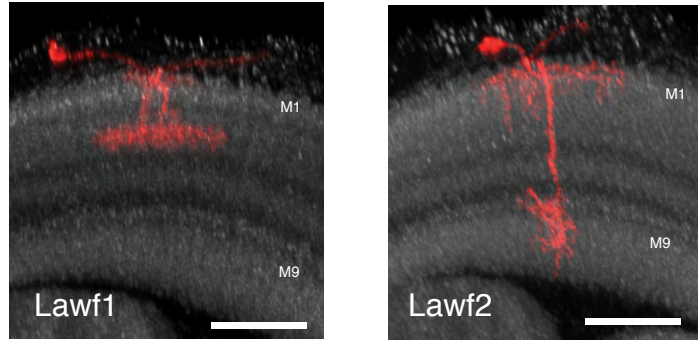
John C. Tuthill, Aljoscha Nern, Gerald M. Rubin, and Michael B. Reiser

Figure S1

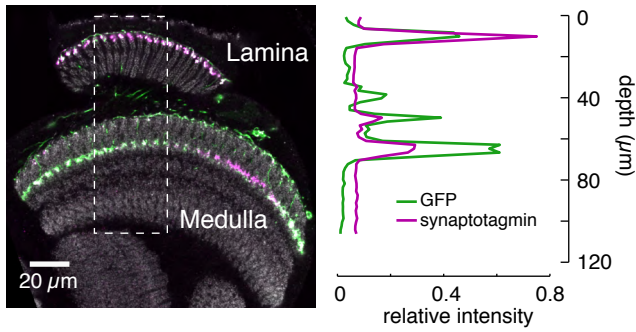
A Stochastically labeled Lawf1 neurons



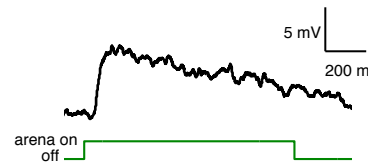
B Lawf1 and Lawf2 have distinct medulla arbor patterns



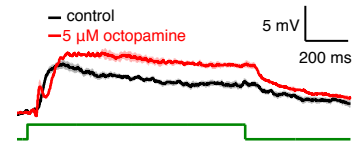
C Lawf1 polarity



D Lawf1 response to light flash



E Octopamine modulates Lawf1 neurons



F Anti-choline acetyltransferase antibody staining of Lawf2

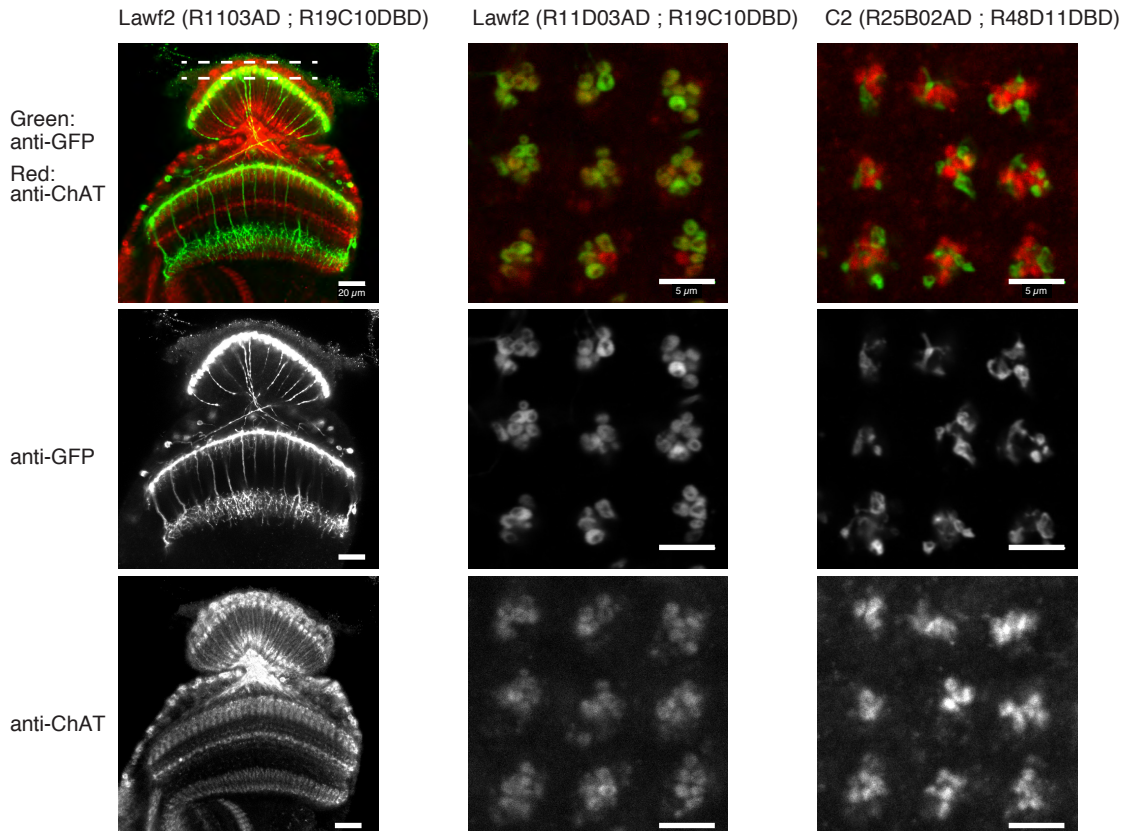


Figure S1, related to Figure 1.

(A) Stochastically-labeled Lawf1 neurons. Single cell flip-outs of two Lawf1 neurons (green) are shown. The entire pattern of the GAL4 line (R11G01) is shown in magenta. The image is a projection of a series of confocal sections. Scale bar represents 20 μm .

(B) Lawf1 and Lawf2 have different layer patterns in the medulla. Scale bar represents 20 μm .

(C) Distribution of an epitope-tagged presynaptic marker (synaptotagmin-HA) in Lawf1 neurons.

(D) Example response of a Lawf1 neuron to a 1s full-field light flash.

(E) Average response of wide-field neurons to brief light flashes (mean \pm s.e.m, n = 4 cells). Unlike Lawf2 neurons, Lawf1 are non-spiking and adapt slowly to static light stimuli. Octopamine increases the amplitude of Lawf1 responses, and introduces a hyperpolarizing transient at light ON.

(F) Anti-choline acetyltransferase antibody staining suggests that Lawf2 neurons release acetylcholine. The left column shows a single confocal section through the lamina and medulla. In the distal lamina, anti-ChAT staining almost completely overlaps with bouton-like terminals of Lawf2 wide-field neurons (center column) but not with terminals of C2 centrifugal neurons (right column). The dashed lines in the left column illustrate the approximate volume of the lamina from which the projection images in the center and right columns were generated. Monoclonal antibody ChAT4B1 was used for anti-ChAT staining (shown in red). Neurons were visualized using R11D03AD; R19C10DBD (Lawf2) and R25B02AD; R48D11DBD (C2) Split- GAL4 lines (Tuthill et al., 2013) and pJFRC12-10XUAS-IVS-myr::GFP as a reporter.

Figure S2

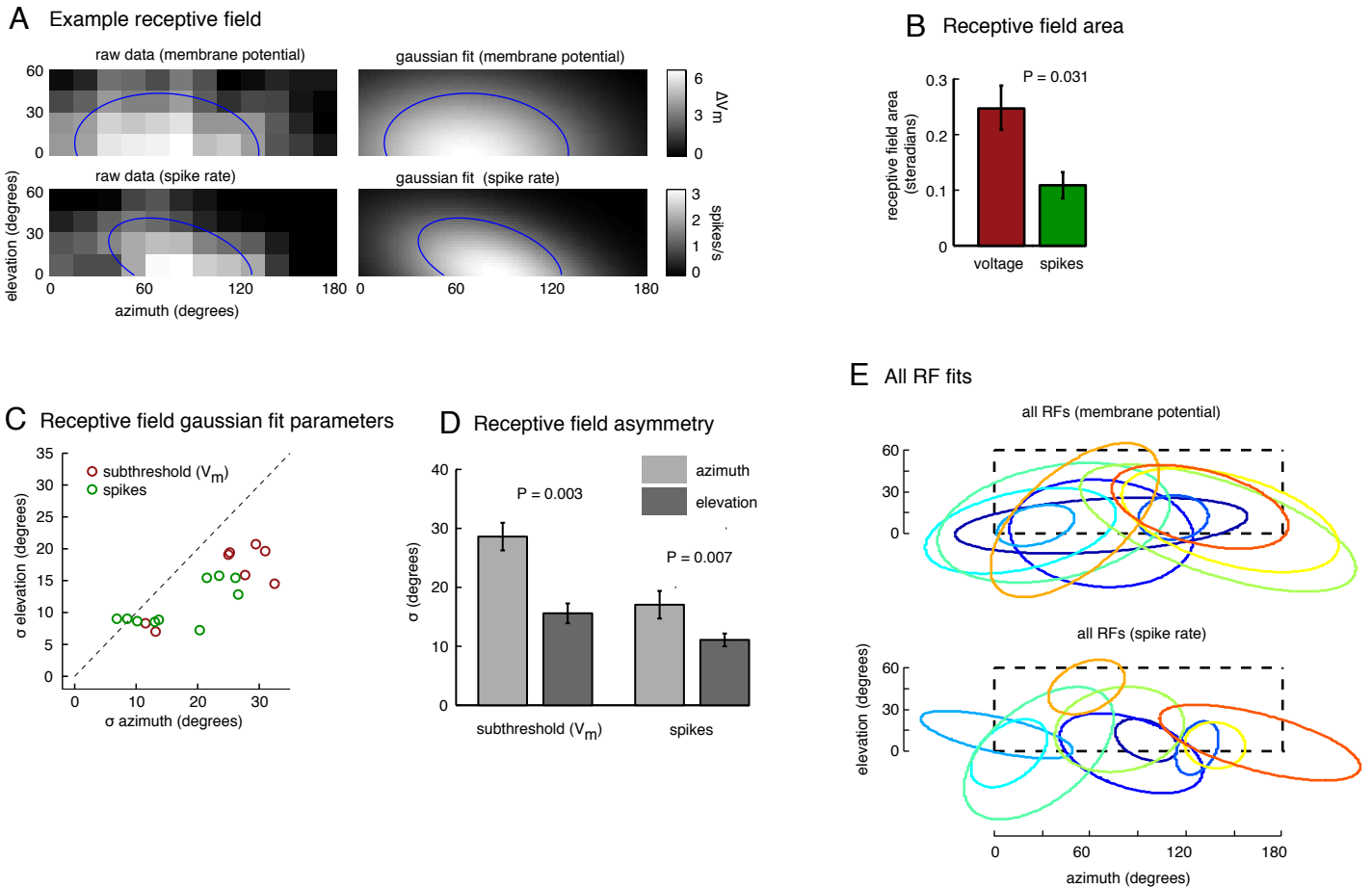


Figure S2, related to Figure 2.

(A) Receptive fields were mapped by flashing bright square stimuli ($30^\circ \times 30^\circ$) at 33 overlapping locations in the arena, and calculating the mean depolarization and spike rate at each point. The spatial profile of each cell was fit to a two-dimensional Gaussian (see Supplemental Experimental Procedures). Left: raw data for means and spike rates of a typical wide-field neuron. Right: Two-dimensional receptive field profiles. In both panels, the blue ellipse represents 1 s.d. of the fit Gaussian. For illustration purposes, this example is the same cell in Figure 2D.

(B) Receptive fields measured by subthreshold activity are significantly larger than those measured by spike rate ($n = 10$ cells).

(C) Distribution of receptive field sizes along the azimuth and elevation of the fly's visual field.

(D) Measured receptive fields were significantly wider in azimuth than elevation, as measured with both subthreshold activity and spike rate. However, this effect may be partially attributed to the dimensions of the arena used to map receptive fields (180° wide \times 60° high), given the relatively uniform distribution of putative dendritic arbors in the medulla (Figure 1C-D).

(E) Outlines of Gaussian fits for all receptive fields measured in the study ($n = 10$ cells). Receptive fields are shown for both mean depolarization (top) and spike rate (bottom), with color indicating cell identity. The dashed box is the outline of the visual arena.

Figure S3

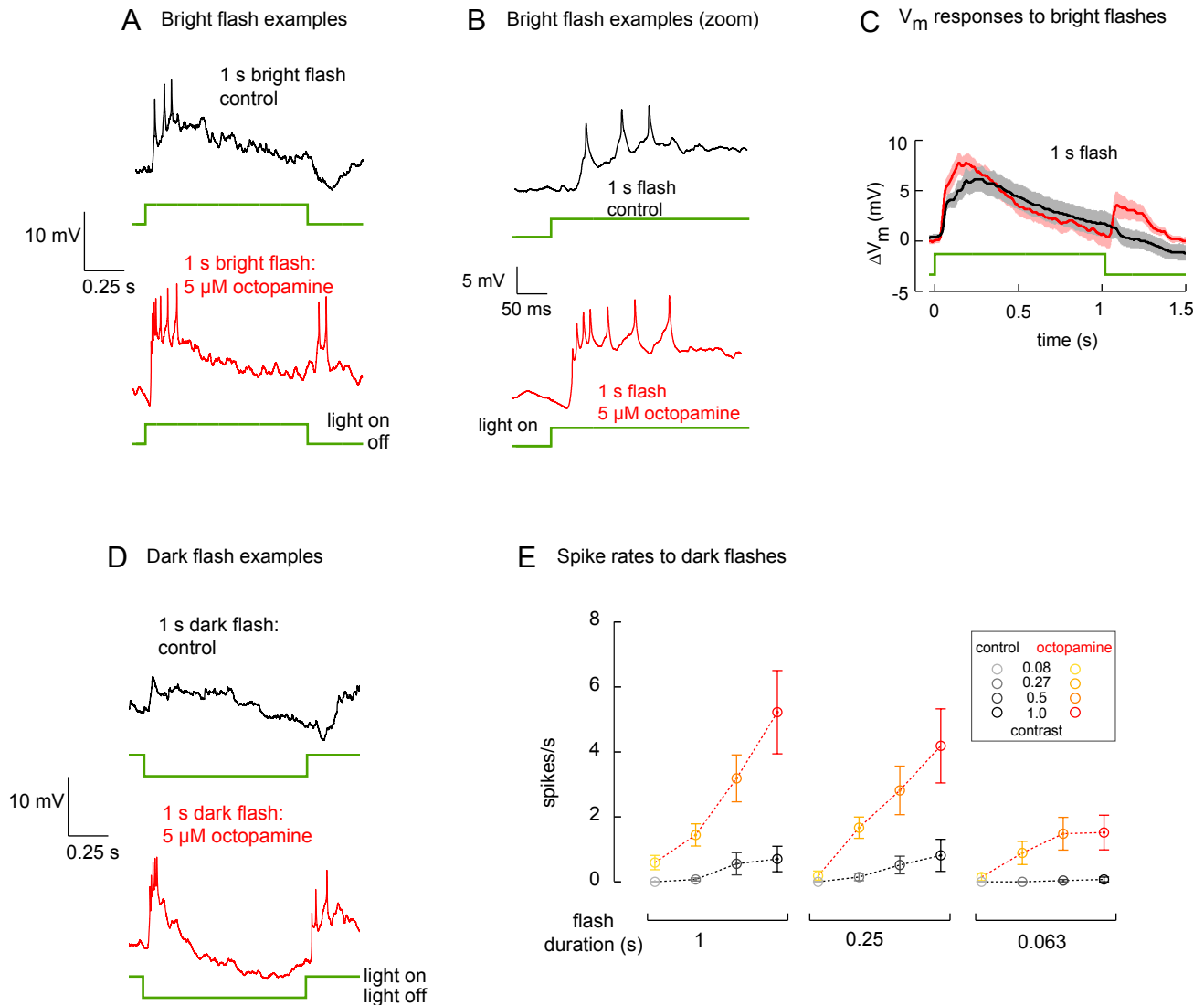


Figure S3, related to Figure 3.

(A) Example traces of a wide-field neuron to a 1 s light increment with and without 5 μ M octopamine in the bath.

(B) Finer timescale of the trace in A, illustrating the long delay between light onset and the response of the neuron. Mean spike latencies across neurons are shown in Figure 3E.

(C) Average membrane potential responses of wide-field neurons to a 1 s light flash (mean \pm s.e.m, $n = 11$ cells). Spikes were removed by low-pass filtering prior to averaging.

(D) Example trace of a wide-field neuron to a 1 s light decrement, with and without 5 μ M octopamine in the bath (same cell as in A).

(E) Spike rates across contrast conditions and flash durations for light off stimuli, calculated across the full stimulus period (1000, 250, or 62.5 ms). Data are from the same cells as in Figure 3D ($n = 11$ cells).

Figure S4

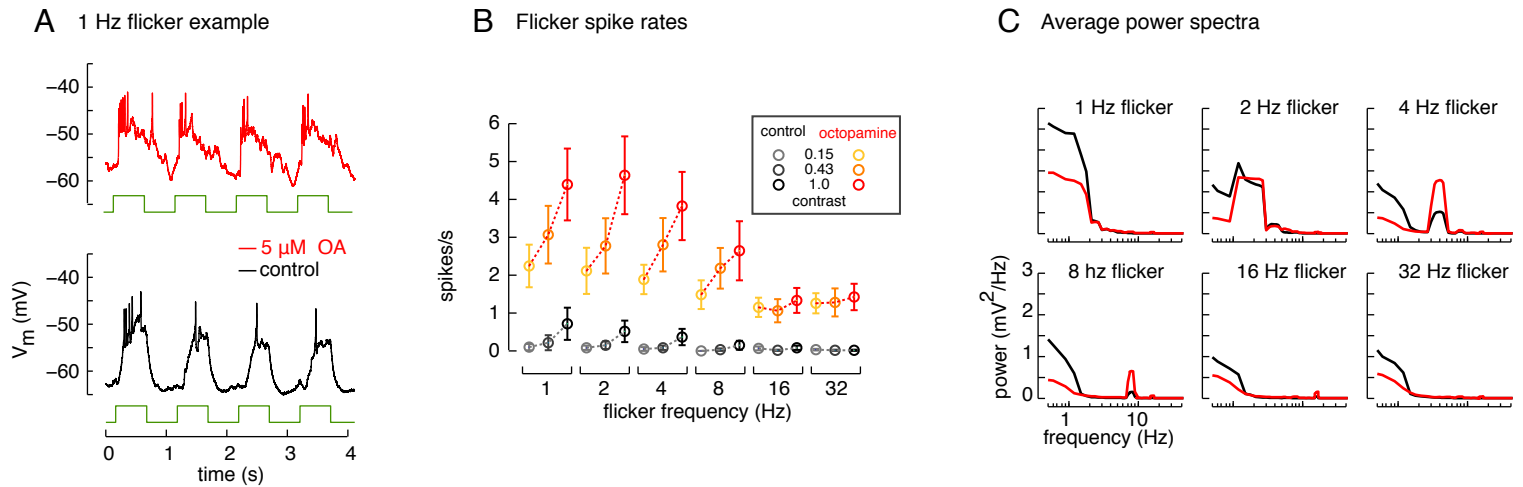


Figure S4, related to Figure 4.

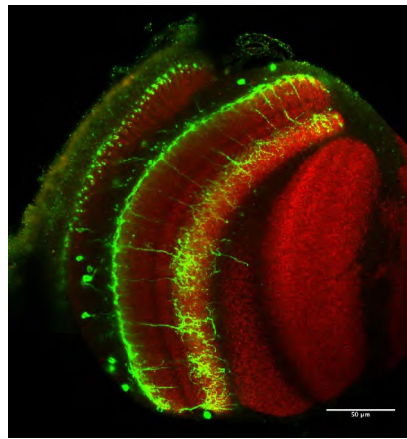
(A) Example traces of a wide-field neuron to a maximum contrast 1 Hz full-field flicker stimulus.

(B) Spike rates across contrast conditions and flicker frequencies, calculated as the average spike frequency across the last 3 s of each 4 s stimulus. The data in the top panel of Figure 4B correspond to the highest contrast condition.

(C) Average power spectra at each flicker frequency (bottom panel of Figure 4B, $n = 10$ cells). Each trial was 4 s long, and repeated twice for each cell. Power spectra of individual traces were calculated from the last 3 s of each trial using multi-taper spectral estimation, and averaged on a per-fly basis (see Supplemental Experimental Procedures for details).

Figure S5

A UAS-GFP-Kir2.1 image

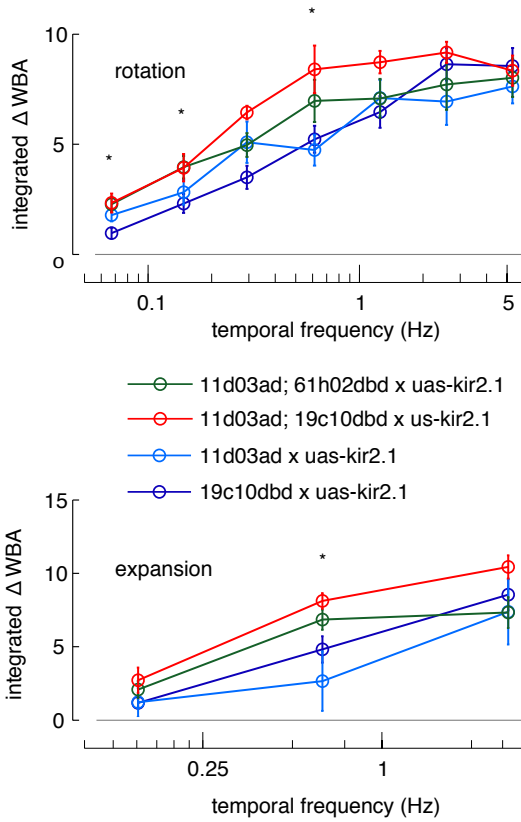


Green:
Lawf2 neurons
(anti-GFP labeling,
UAS Kir2.1GFP reporter)

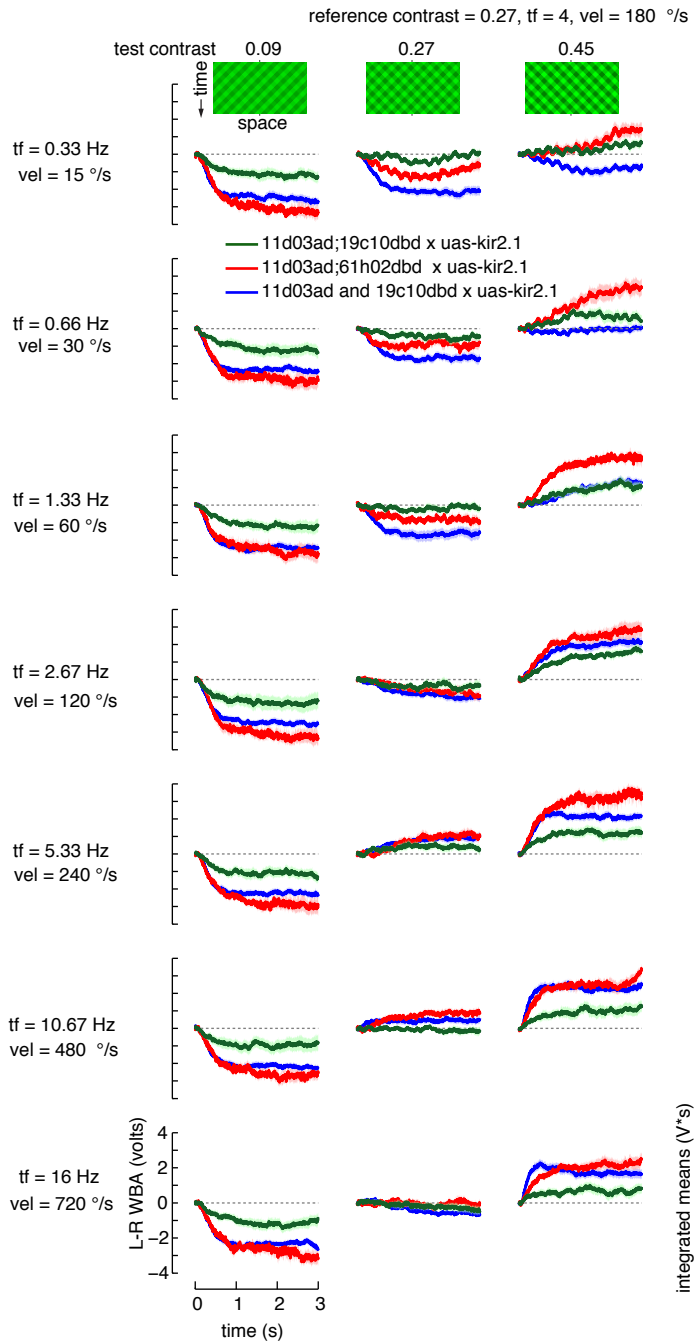
Red:
Presynaptic marker
(anti-Brp labeling,
Nc82 mAb)

R11D03AD R19C10DBD

B basic optomotor responses



C motion nulling time series



D motion nulling means and fits

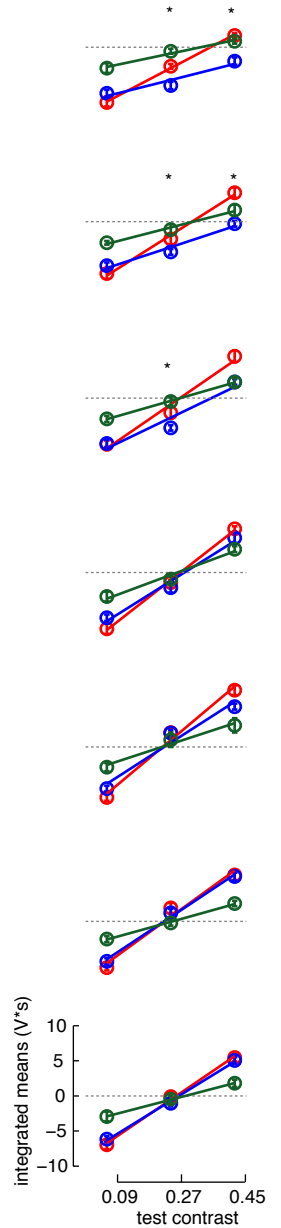


Figure S5, related to Figure 5.

(A) UAS-EGFP-Kir2.1 expressing wide-field cells show normal overall morphology. The image shows the optic lobe pattern of the R11D03AD R19C10DBD Split-GAL4 line with additional labeling of a presynaptic marker (anti-Brp, Nc82 mAb). Kir2.1 expression also abolished Lawf2 spiking, hyperpolarized the resting potential, and decreased the input resistance (Tuthill et al, 2013).

(B) Behavioral effects of silencing wide-field neurons. Two Split-GAL4 lines (red and green), both targeting Lawf2 neurons, were compared to the mean of two control genotypes (blue and purple) possessing only one of the two Split-GAL4 transgenes. The data in Fig. 5C,D are from the same dataset, except that the two experimental and control genotypes are averaged in the primary figure (for visualization only, statistical significance was determined as described in the Supplemental Experimental Procedures). Flies were tested with full-field motion stimuli, traditionally referred to as the 'optomotor' stimulus (test velocities = 7.5, 15, 30, 60, 120, 240, and 480 °/s; $\lambda = 90^\circ$). The integrated Δ WBA was calculated by integrating the area under each turn response, and data are plotted as means \pm s.e.m ($n \geq 12$ for each genotype). The expansion stimulus is similar to wide-field rotation, except the front and rear of the arena move in opposite directions, creating a lateral focus of expansion (Tammero et al., 2004). Asterisks indicate that both experimental genotypes are significantly different from the control (* $P < 0.05$, un-paired t-tests corrected for FDR).

(C) Fly responses to motion nulling stimuli. As before, two Split-GAL4 lines (red and green), both targeting Lawf2 neurons, were compared to the mean of two control genotypes (blue) possessing only one of the two Split-GAL4 transgenes. Time series represent mean turning behavior of at least 12 flies of each genotype (\pm s.e.m) in response to open-loop rotation of two superimposed square-wave gratings ($\lambda = 45^\circ$): a constant reference stimulus, and a test stimulus whose contrast is varied across trials (Figure 5E). At low test contrast, control flies turn in the direction of the reference stimulus (Δ WBA > 0); at high test contrast, flies attempt to follow the reference stimulus (Δ WBA < 0). Space-time diagrams are for reference and test stimuli moving at the same velocity, to emphasize contrast differences.

(D) Mean integrated responses of the behavioral time series (* $P < 0.05$, un-paired t-tests corrected for FDR; see Supplemental Experimental Procedures for details). A line is fit through each series of tests contrasts to determine the zero crossing, or "null contrast"—the contrast of the test stimulus needed to cancel, or null, the reference stimulus (Figure 5E). The contrast sensitivity in Figure 5F is the inverse of the null contrast (at each temporal frequency) averaged across the two experimental genotypes.

Supplemental Experimental Procedures

Fly Stocks. Split-GAL4 (Luan et al., 2006; Pfeiffer et al., 2010) lines were constructed as described (Tuthill et al., 2013). Two Split-GAL4 lines were used to target wide-field neurons: R11D03AD;R19C10DBD and R11D03AD;R61H02DBD (Tuthill et al., 2013). Other GAL4 and Split-GAL4 drivers used are R11D03, a GAL4-line that labels Lawf2, R11G01, which labels Lawf1, a Lawf1-specific Split-GAL4 line, R11G01AD; R15G08DBD, and a C2-specific Split-GAL4 line, R25B02AD;R48D11DBD (Tuthill et al., 2013). For electrophysiology experiments, R11D03AD;R19C10DBD was crossed to pJFRC7-20XUAS-IVS-mCD8::GFP or pJFRC12-10XUAS-IVS-myr::GFP (Pfeiffer et al., 2010). No differences were observed between the two and data were pooled. For neural silencing experiments, each line was crossed to w^+ ; tubP-GAL80^{ts}; UAS-Kir2.1-GFP flies, backcrossed ten generations into a wild-type genetic background (Tuthill et al., 2013). Because GAL80^{ts} does not bind to split-GAL4 proteins with a p65-AD, the GAL80^{ts} protein had no effect on the expression of the Split-GAL4 lines used. All flies for behavior and electrophysiology were kept in a 25° incubator on a 14 h:10 h light:dark cycle, and tested within a 4 hour window prior to lights off.

Histology and anatomical analyses. Indirect immunofluorescence of fly brains was performed as previously described (Tuthill et al., 2013), with brains fixed in 2% formaldehyde in PBS for 1 hr at room temperature. Primary antibodies used were mouse monoclonal antibody (mAb) ChAT4B1 (DSHB; dilution 1:100) (Takagawa and Salvaterra, 1996), mouse mAb Nc82 (DSHB, dilution 1:50) (Wagh et al., 2006), anti-GFP rabbit polyclonal (Invitrogen, A11122, 1:1000 dilution) and anti-mCD8a rat mAb (Invitrogen, MCD0800, 1:100 dilution). Secondary antibodies were from Invitrogen. Samples were imaged on a Zeiss LSM710 confocal microscope with 20x 0.8 NA, 40x 1.3 NA or 63x 1.4 NA objectives. A “flip-out”-based approach (Struhl and Basler, 1993) was used for stochastic single cell labeling with one or more colors. The detailed methodology for multicolor labeling will be described elsewhere (Nern et al, in

preparation). Single cell labeling shown in Figure 1B and Figure S1 used pBPhsFlpPEST-Opt in attP3 (a gift from Barret Pfeiffer, Rubin lab) as Flp source, pJFRC41-10XUAS-FRT>STOP>FRT-myr::GFP in attP40 (Pan et al., 2012) as a stop-cassette reporter and pJFRC21-10XUAS-IVS-mCD8::RFP in attP2 (Pfeiffer et al., 2010) to reveal the entire GAL4-line pattern. pBPhsFlpPEST-Opt is identical to pBPhsFlp1 but contains codon optimized Flp2PEST instead of Flp1 in pBPhsFlp1 (Nern et al., 2011). Additional images of single wide-field neurons (Figure 1C, Figure S1B, and images used for quantification of Lawf2 arbor sizes) were obtained by screening the optic lobe dataset of the Janelia Fly Light Single Neuron Project. Individual neurons from the FlyLight images were segmented using NeuronSeparator (Myers et al, unpublished) and rotated views generated using NeuronAnnotator (Janelia Fly Light Scientific Computing Team, unpublished), a modified version of Vaa3D (Peng et al., 2010). Column spread of wide-field neuron processes was calculated by comparing the average area of a medulla column to the 2-dimensional area of wide-field neuron arborizations in the medulla. For each brain, the average area of a medulla column was estimated by manually drawing polygons around ten individual columns of the reference pattern in medulla layer M9. Convex hulls were then fit to the projections of wide-field neuron arborizations in layers M1 and M8/M9/M10. To estimate column coverage, the area of each convex hull was divided by the average column area. In the lamina, the reference pattern allowed clear differentiation of individual columns within the same projection plane as the labeled wide-field neuron. Axonal arbors in the lamina innervated 28 ± 1.5 cartridges (mean \pm s.e.m.; $n = 8$ cells), while arbors in M1 innervated 121 ± 11 cartridges ($n = 5$), and M8-10 17 ± 2 cartridges ($n = 5$). Coverage estimates provided in the text are based on cell body counts of 134, 137, 147 cells, counted manually from 20X confocal stacks of 3 brains. We measured arbor symmetry in the lamina and medulla by fitting an ellipse to the outline of each neuronal arbor and measuring the angle of the major axis. The Lawf2 axonal arbors in the lamina were significantly skewed along the dorsal-ventral axis, with a mean orientation angle of $91^\circ \pm 1.8^\circ$ (where the dorsal axis is 90°), measured from 8 cells ($p < 0.001$, Rayleigh test). Image processing analysis was done using Fiji (<http://fiji.sc/>) and figures were assembled in

Adobe InDesign and Adobe Illustrator.

For the synaptotagmin images in Figure 1E and Figure S1C, Lawf2 and Lawf1 specific split GAL4 lines (R11D03AD; R19C10DBD and R11G01AD; R15G08DBD) were used to drive expression of an HA-epitope-tagged synaptotagmin (Zhang et al., 2002) and a FLAG-tagged membrane-targeted GFP. Detailed constructs will be described elsewhere (Nern et al, in preparation). Primary antibodies were a rabbit anti-HA monoclonal (HA-Tag; Cell Signaling Technology; dilution 1:300) and a rat anti-FLAG monoclonal antibody (DYKDDDDK Epitope Tag Antibody L5; Novus Biologicals; 1:200). The histograms show the synaptotagmin and GFP signals for each row in the corresponding images, smoothed using a moving average across 10 neighboring pixels. GFP and synaptotagmin signals were normalized to the maximum signal in each channel prior to averaging.

Electrophysiology. Whole-cell patch clamp recordings were made from GFP-labeled neurons in intact flies. 2-3 day old female flies were anesthetized on a Peltier device at 2°C and fixed to a custom-milled steel holder with UV-activated glue. The proboscis was fixed to the head capsule with a tiny drop of glue. After manual dissection of a small region of the dorsal cuticle with fine forceps, the perineural sheath covering the medulla was ruptured by local application of collagenase diluted in extracellular saline (0.5 mg ml⁻¹), similar to a previously described technique (Maimon et al., 2010). In brief, a small patch of the sheath was sucked into a micropipette (2-4 μm tip) containing collagenase solution for ~30 seconds, while the bath was held at 29°C. When positive pressure was applied to the pipette, the sheath would rupture, exposing the underlying cell bodies. At this point, the bath temperature was lowered to 20°C to match the temperature under which we performed behavior experiments.

The brain was continuously perfused (at a rate of 1 mL/min) with an extracellular saline solution containing (in mM): 103 NaCl, 3 KCl, 5 N-Tris(hydroxymethyl)methyl-2-aminoethane-sulfonic acid, 8 trehalose, 10 glucose, 26 NaHCO₃, 1 NaH₂PO₄, 1.5 CaCl₂, and 4 MgCl₂, adjusted to 267–269 mOsm (Wilson and Laurent, 2005). The saline was bubbled with 95% O₂/5% CO₂ gas for a final pH of 7.3. Pressure-polished patch-clamp

electrodes (9-12 M Ω) contained (in mM) 140 potassium-aspartate, 1 KCl, 10 HEPES, 1 EGTA, 0.5 Na₃GTP, and 4 MgATP, adjusted to pH 7.3, 265 mOsm (Wilson and Laurent, 2005). We sometimes included 10 μ M Alexa Fluor 568 hydrazide (Invitrogen) in the intracellular solution for visualization purposes. Stock solutions of octopamine hydrochloride (Sigma) and CdCl₂ (Sigma) were added to the saline reservoir to achieve final concentrations of 5 and 200 μ M, respectively.

Recordings were obtained from wide-field neuron cell bodies under visual control using a Nikon Eclipse FN1 microscope with a 60X water-immersion objective. The sub-stage optics were removed to position the visual arena, and high contrast images of the brain were attained with diffuse illumination via an adjustable infrared LED placed below the fly (this same LED was also used to illuminate the fly during flight experiments). The fly was precisely positioned with two cameras (Firefly MV 0.3 MP; Point Grey), one of which was also used to monitor behavior during flight. Online image processing (at 60 Hz) to detect flight was performed with custom Matlab code and recorded simultaneously with electrophysiological data.

All recordings included in our analysis were made from the right side of the brain, and one cell was recorded in each fly. To prevent fly movement and reduce neural response variability, the legs and wings were glued in all experiments except those when the fly was flying (Figure 3A-C). The fact that the legs were not glued during recordings from flying flies likely contributed to the increased gain of responses during non-flight epochs (e.g., Figure 3A). Overall, neurons recorded from unrestrained flies had a higher response gain than those from restrained flies; for example, the spike latency of unrestrained flies (Figure 3C) was lower than that of restrained flies (Figure 3E).

Current-clamp recordings were low-pass filtered at 5 kHz using an Axopatch 200B amplifier, and digitized at 10 or 20 KHz using either a Digidata 1440A data acquisition board (DAQ) and Axoscope software (Molecular Devices), or a National Instruments DAQ (X-series, USB-6343) and custom Matlab code. Current injection experiments were executed with Matlab control of the National Instruments DAQ. All traces are corrected for an experimentally measured liquid junction potential of 12 mV. In most

cells, we injected a small constant hyperpolarizing current (0–10 pA) to compensate for seal conductance (Gouwens and Wilson, 2009; Wilson and Laurent, 2005). At the onset of each experiment, including those in Figure 4C-D, the membrane potential was set to an initial value of -62 mV, and membrane potential and input resistance were monitored throughout.

Though wide-field neurons were typically silent at rest, 15 out of 24 cells exhibited slow spontaneous oscillations in darkness that were greater than 2.5 mV peak-to-peak. In all cases, oscillations were abolished by light exposure, or application of 1 μ M TTX. The mean oscillation frequency was 0.35 Hz, and the mean peak-to-peak amplitude was 8.70 mV.

The display used in electrophysiology experiments was a half-cylinder variant of the green (peak: 565 nm) visual arena described previously (Reiser and Dickinson, 2008). The physiology arena covered 180° x 60° of the fly's visual field, with each of the 96 x 32 LEDs subtending an angle of \sim 1.875° on the fly eye. The maximum intensity of the arena (15/15) was approximately 72 cdm^{-2} and minimum intensity (0/15) was 0 cdm^{-2} , with intermediate grayscale values distributed linearly within this range. More information is available at <http://flypanels.org/>.

All analyses of electrophysiology data were performed in Matlab. Spikes were detected by high-pass filtering raw signals, then identifying peaks that rose above an amplitude threshold. The variability in size and duration of spikes in our recordings are typical of patch-clamp recordings from *Drosophila* neurons, and are likely due to electrotonic filtering between the spike initiation zone and cell body, as well as variability in recording conditions. Application of 1 μ M TTX reliably abolished all spiking activity in wide-field neurons (data not shown). Example traces in all figures were not filtered following digitization, and group data are reported as mean values, averaged across experiments, \pm s.e.m. Statistical tests are paired *t* tests, unless otherwise indicated. In Figure 4B and Figure S4, power at the flicker frequency was calculated using multi-taper spectral estimation procedures implemented with the Chronux toolbox for Matlab

(<http://chronux.org/>)(Bokil et al., 2010). In all spectral analyses, we used a time-bandwidth product of 3 and 5 tapers.

Because Lawf2 neurons did not respond to small spots, receptive fields were mapped by flashing square stimuli (30° x 30°) at 33 overlapping locations in the arena (0.5 s flashes at a rate of 1 Hz), and calculating the mean depolarization and spike rate at each point in the arena (Figure 2D and Figure S2). The spatial profile of each cell was fit with a two-dimensional Gaussian given by the function:

$$Ae^{-\left[\frac{(u-u_0)^2}{\sigma_u^2} + \frac{(v-v_0)^2}{\sigma_v^2}\right]}$$

where u and v are the long and short axes rotated by an orientation angle (θ),

$$u = \cos(\theta) x + \sin(\theta) y, \quad v = -\sin(\theta) x + \cos(\theta) y,$$

and σ_u and σ_v are the standard deviations of Gaussians. Because receptive fields were very large, they often extended beyond the boundaries of the visual arena. For the analysis in Figure S2D-G, we used only those cells in which the receptive field peak was on the arena; the two-dimensional Gaussian fits for all these cells are shown in Figure S2G. For the experiments in Figure 2E, in which stimuli of different sizes were used to examine size selectivity, each stimulus was centered on the previously mapped receptive field. To increase the amplitude of light-evoked responses, the experiments in Figure 2E were performed with 5 μ M octopamine in the bath. In Figure 2E, we approximated the spherical angle subtended on the fly's eye as $hw/(180^\circ)^2$, where h and w are the stimulus height and width in degrees.

Tethered flight. Flight behavior experiments and data analysis were conducted as previously described (Tuthill et al., 2013). The visual arena consisted of a 32x88 array of green LEDs covering 330° in azimuth and 120° in elevation (Reiser and Dickinson, 2008). Within the arena, the position of the wings was monitored using an analog optical wingbeat analyzer (Gotz, 1987). In all figures showing open-loop flight behavior, we follow a convention of plotting the turning response of flies as the left minus right wing

beat amplitude (Δ WBA), a measure which is directly proportional to yaw torque (Tammero et al., 2004). Half of the conditions (e.g., CCW rotation) were inverted and averaged with the corresponding symmetric conditions (e.g., CW rotation).

The rotation stimuli in Figure 5C-D were square wave gratings of alternating bright (intensity = 72 cdm^{-2}) and dark (intensity = 0) stripes with a spatial period, λ , of 90° (one period consists of a dim and a bright bar, each 12 pixels wide). Importantly, these stimuli did not saturate fly steering responses, as we frequently observed larger responses measured under identical conditions (Tuthill et al., 2013).

The motion nulling paradigm was adapted from previous studies of contrast sensitivity in humans (Cavanagh and Anstis, 1991) and zebrafish (Smear et al., 2007) (Figure 5E-F and Figure S5C-D), and was recently employed in another study of fly behavior (Tuthill et al., 2013). Each trial consisted of two superimposed gratings ($\lambda=45^\circ$, mean luminance = 24.8 cdm^{-2}): a constant reference grating (contrast = 0.27), and one of three test gratings (contrast = 0.09, 0.27, or 0.5). The reference grating always rotated at $180^\circ/\text{s}$, while test gratings rotated at one of seven velocities (15, 30, 60, 120, 240, 480, 720 $^\circ/\text{s}$). The null contrast is the point at which the two superimposed gratings are not distinguished, and the mean response of the fly is zero. Because the reference pattern remained constant (4 Hz), peak contrast sensitivity occurred when the reference and test pattern were moving close to the same speed. Null contrasts were calculated as the zero-crossing of a line fit through the three response values at each velocity of the test stimulus (Figure 5E). These fit lines are shown in Figure S5D. The error bars in Figure 5F were calculated by fitting lines through the upper and lower standard error values of each motion nulling trial. However, statistical tests were performed on individual conditions, as indicated in Figure S5D.

As in a previous study of tethered flight behavior using the Split-GAL4 system (Tuthill et al., 2013), we compared the behavioral responses of the two Lawf2 Split-GAL4 lines crossed to UAS-Kir2.1 to the responses of two control lines (each an individual Split-GAL4 AD or DBD alone, also crossed to UAS-Kir2.1). The behavioral responses of these control lines (11D03AD x UAS-Kir2.1 and 19C10DBD x UAS-Kir2.1) were pooled

for further analysis (but are shown individually for the optomotor responses in Figure S5B). We averaged behavioral data from the two experimental lines and the two control lines to produce the time series and means presented in Figure 5. For the contrast nulling experiments, the mean data from the individual Split-GAL4 lines are included in Figure S5C-D. To determine statistical significance, un-paired t-tests were performed on the mean turning amplitudes of each genotype. For each stimulus condition, a result was considered significant only if both split-GAL4 lines were statistically different from the mean response of the 2 control lines. We controlled for multiple comparisons across all behavioral experiments using false discovery rate (FDR) correction, so P-values reported in the text correspond to equivalent q-values as defined by Benjamini and Hochberg (Benjamini and Hochberg, 1995).

Model and Simulation. We modeled a local lamina circuit as a series of linear filters beneath simple compound eye optics. For the point-spread function of an ommatidial lens we used Gaussian sampling:

$$L(\theta) = k \exp \left[\frac{4 \ln 2}{\Delta p^2} \theta^2 \right]$$

where k is a standardization constant, Δp is the 5° acceptance angle of the photoreceptor (Heisenberg and Wolf, 1984), and θ is the vector of discrete positions through a pair of ommatidia with increments of 0.375° . We used an interommatidial angle ($\Delta\phi$) of 4.5° (Snyder, 1979). The image was formed by the convolution of an intensity signal, $I(\theta, n)$, a function of angular position (θ) and the discrete sample time (n), with the acceptance angle of the ommatidia. We then used ray tracing to simulate the view of six neighboring ommatidia in front of our standard cylindrical LED display. The lamina model computed the local optic flow field from the resulting retinal image.

For simplicity, the temporal properties of the photoreceptors and LMCs were modeled as a single first-order linear low-pass filter with a time constant of $\tau_{pr} = 8$ ms. This value was previously used (Lindemann et al., 2005) as an approximation for the photoreceptor corner frequency measured with white-noise luminance fluctuations in the blowfly (van

Hateren and Snippe, 2001). Although complex filter kernels more closely approximate the LMC response (James, 1992), we chose this basic model for 2 reasons (1) the simple linear model provides an intuitive method for understanding the role of wide-field neuron feedback, and (2) measured LMC responses may contain components of wide-field neuron feedback that are impossible to dissociate from intrinsic LMC signals.

We modeled the wide-field neuron as a first-order low-pass filter with a time constant $\tau_{wf} = 24$ ms. This time constant was derived from an exponential fit to the falling phase of the membrane potential frequency tuning curve in Figure 4B (i.e., all points above 1 Hz), and corresponds to wide-field neuron behavior in the presence of octopamine (mimicking flight conditions). Simulations using the time constant fit to membrane potential responses without octopamine ($\tau_{wf} = 42$ ms) qualitatively matched these, with small temporal differences.

Filtered wide-field neuron feedback, with one wide-field neuron pooling signals from six model ommatidia, was subtracted from incoming luminance signals at the “feedback integration” stage of each model lamina unit (Figure 6A). The model consisted of 36 model ommatidia and 6 model wide-field neurons, and each ommatidial unit received feedback from three neighboring wide-field neurons. Using larger arrays of model ommatidia with connections numerically matched to those measured anatomically did not qualitatively affect the results of the simulation.

In Figure 6B, the input to the model was 100 s of naturalistic time series data (van Hateren, 1997) kindly provided by Hans van Hateren. The spectral power of model output signals was calculated using Welch’s method. In Figure 6C, the output of the lamina model, presented with moving grating stimuli identical to those used in the behavioral experiments of Figure 5D, was passed through an array of Hassenstein Reichardt elementary motion detectors (EMDs; Hassenstein and Reichardt, 1956). The structure and parameters of the EMD model were identical to a previous study of optomotor behavior in the flight arena (Tuthill et al., 2011): we used an EMD time constant of 20 ms, and a slight gain imbalance (1%) prior to the subtraction stage of the EMD model (Tuthill et al., 2011). The model responses were integrated across 36 model

ommatidia, and response amplitudes were normalized to the peak amplitude of the temporal frequency tuning curve for each of the 2 conditions (with and without wide-field feedback).

Supplemental references

- Benjamini, Y., and Hochberg, Y. (1995). Controlling the False Discovery Rate: A Practical and Powerful Approach to Multiple Testing. *J R Stat Soc Ser B-Methodol* 57, 289-300.
- Bokil, H., Andrews, P., Kulkarni, J.E., Mehta, S., and Mitra, P.P. (2010). Chronux: a platform for analyzing neural signals. *Journal of neuroscience methods* 192, 146-151.
- Cavanagh, P., and Anstis, S. (1991). The contribution of color to motion in normal and color-deficient observers. *Vision Res* 31, 2109-2148.
- Gotz, K.G. (1987). Course-Control, Metabolism and Wing Interference During Ultralong Tethered Flight in *Drosophila Melanogaster*. *J Exp Biol* 128, 35-46.
- Gouwens, N.W., and Wilson, R.I. (2009). Signal propagation in *Drosophila* central neurons. *J Neurosci* 29, 6239-6249.
- Hassenstein, V.B., and Reichardt, W. (1956). Systemtheoretische Analyse der Zeit-, Reihenfolgen- und Vorzeichenauswertung bei der Bewegungsperezeption des Russelkafers *Chlorophanus*. *Z Naturforsch* 11 b, 513-524.
- Heisenberg, M., and Wolf, R. (1984). *Vision in Drosophila: Genetics of Microbehavior* (Berlin: Springer-Verlag).
- James, A.C. (1992). Nonlinear operator network models of processing in the fly lamina. In *Determination of neural receptive fields, function and networks*, R. Pinter, and B. Nabet, eds. (Boca Raton, FL.: CRC), pp. 39-73.
- Lindemann, J.P., Kern, R., van Hateren, J.H., Ritter, H., and Egelhaaf, M. (2005). On the computations analyzing natural optic flow: quantitative model analysis of the blowfly motion vision pathway. *J Neurosci* 25, 6435-6448.
- Luan, H., Peabody, N.C., Vinson, C.R., and White, B.H. (2006). Refined spatial manipulation of neuronal function by combinatorial restriction of transgene expression. *Neuron* 52, 425-436.
- Maimon, G., Straw, A.D., and Dickinson, M.H. (2010). Active flight increases the gain of visual motion processing in *Drosophila*. *Nat Neurosci* 13, 393-399.
- Nern, A., Pfeiffer, B.D., Svoboda, K., and Rubin, G.M. (2011). Multiple new site-specific recombinases for use in manipulating animal genomes. *Proc Natl Acad Sci U S A* 108, 14198-14203.
- Pan, Y., Meissner, G.W., and Baker, B.S. (2012). Joint control of *Drosophila* male courtship behavior by motion cues and activation of male-specific P1 neurons. *Proc Natl Acad Sci U S A* 109, 10065-10070.

Peng, H., Ruan, Z., Long, F., Simpson, J.H., and Myers, E.W. (2010). V3D enables real-time 3D visualization and quantitative analysis of large-scale biological image data sets. *Nature biotechnology* 28, 348-353.

Pfeiffer, B.D., Ngo, T.T., Hibbard, K.L., Murphy, C., Jenett, A., Truman, J.W., and Rubin, G.M. (2010). Refinement of tools for targeted gene expression in *Drosophila*. *Genetics* 186, 735-755.

Reiser, M.B., and Dickinson, M.H. (2008). A modular display system for insect behavioral neuroscience. *Journal of neuroscience methods* 167, 127-139.

Smear, M.C., Tao, H.W., Staub, W., Orger, M.B., Gosse, N.J., Liu, Y., Takahashi, K., Poo, M.M., and Baier, H. (2007). Vesicular glutamate transport at a central synapse limits the acuity of visual perception in zebrafish. *Neuron* 53, 65-77.

Snyder, A.W. (1979). Physics of vision in compound eyes. In *Handbook of Sensory Physiology*, H. Autrum, ed. (Berlin: Springer), pp. 225-313.

Struhl, G., and Basler, K. (1993). Organizing activity of wingless protein in *Drosophila*. *Cell* 72, 527-540.

Takagawa, K., and Salvaterra, P. (1996). Analysis of choline acetyltransferase protein in temperature sensitive mutant flies using newly generated monoclonal antibody. *Neuroscience research* 24, 237-243.

Tammero, L.F., Frye, M.A., and Dickinson, M.H. (2004). Spatial organization of visuomotor reflexes in *Drosophila*. *J Exp Biol* 207, 113-122.

Tuthill, J.C., Chiappe, M.E., and Reiser, M.B. (2011). Neural correlates of illusory motion perception in *Drosophila*. *Proc Natl Acad Sci U S A* 108, 9685-9690.

Tuthill, J.C., Nern, A., Holtz, S.L., Rubin, G.M., and Reiser, M.B. (2013). Contributions of the 12 neuron classes in the fly lamina to motion vision. *Neuron* 79, 128-140.

van Hateren, J.H. (1997). Processing of natural time series of intensities by the visual system of the blowfly. *Vision research* 37, 3407-3416.

van Hateren, J.H., and Snippe, H.P. (2001). Information theoretical evaluation of parametric models of gain control in blowfly photoreceptor cells. *Vision Res* 41, 1851-1865.

Wagh, D.A., Rasse, T.M., Asan, E., Hofbauer, A., Schwenkert, I., Durrbeck, H., Buchner, S., Dabauvalle, M.C., Schmidt, M., Qin, G., *et al.* (2006). Bruchpilot, a protein with homology to ELKS/CAST, is required for structural integrity and function of synaptic active zones in *Drosophila*. *Neuron* 49, 833-844.

Wilson, R.I., and Laurent, G. (2005). Role of GABAergic inhibition in shaping odor-evoked spatiotemporal patterns in the *Drosophila* antennal lobe. *J Neurosci* 25, 9069-9079.

Zhang, Y.Q., Rodesch, C.K., and Broadie, K. (2002). Living synaptic vesicle marker: synaptotagmin-GFP. *Genesis* 34, 142-145.